Cell

Bat-infecting merbecovirus HKU5-CoV lineage 2 can use human ACE2 as a cell entry receptor

Graphical abstract

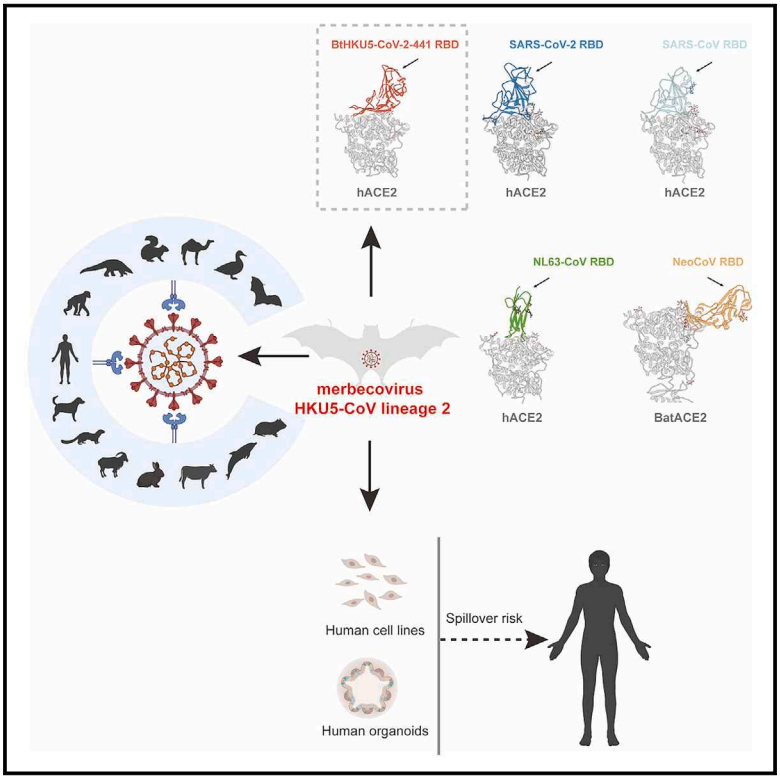

Highlights

- A distinct HKU5 coronavirus lineage (HKU5-CoV-2) is discovered in bats
- Bat HKU5-CoV-2 uses human ACE2 receptor and ACE2 orthologs from multiple species
- Bat HKU5-CoV-2 RBD engages human ACE2 with a distinct binding mode from other CoVs
- Bat HKU5-CoV-2 was isolated and infect human-ACE2-expressing cells

Authors

Jing Chen, Wei Zhang, Yang Li, ..., Peng Zhou, Wei Peng, Zheng-Li Shi

Correspondence

zhanglb@giz.gd.cn (L.Z.), huanyan@whu.edu.cn (H.Y.), zhou_peng@gzlab.ac.cn (P.Z.), peng_wei@gzlab.ac.cn (W.P.), shi_zhengli@gzlab.ac.cn (Z.-L.S.)

In brief

Coronaviruses of the merbecovirus family have been thought to enter cells by using the host cell receptor DPP4. This study identifies a merbecovirus from *Pipistrellus* bats that is capable of entering cells from other mammals via ACE2, and it describes the structural basis for HKU5 interaction with human ACE2.

Chen et al., 2025, Cell *188*, 1–14
March 20, 2025 © 2025 Elsevier Inc. All rights are reserved, including those for text and data mining, AI training, and similar technologies.
https://doi.org/10.1016/j.cell.2025.01.042

Please cite this article in press as: Chen et al., Bat-infecting merbecovirus HKU5-CoV lineage 2 can use human ACE2 as a cell entry receptor, Cell (2025), https://doi.org/10.1016/j.cell.2025.01.042

Cell

CellPress

Article

Bat-infecting merbecovirus HKU5-CoV lineage 2 can use human ACE2 as a cell entry receptor

Jing Chen,[1,8] Wei Zhang,[2,3,8] Yang Li,[1,8] Chen Liu,[4,8] Tianyi Dong,[1,5] Huiyu Chen,[2,3] Chunguang Wu,[1,5] Jia Su,[1,5] Bei Li,[1] Wei Zhang,[1] Ben Hu,[1] Jingkun Jia,[1,5] Cheng-Bao Ma,[4] Yan Zhu,[1] Xiangyang He,[6] Ang Li,[2,3] Kaiyi Pan,[1,5] Haofeng Lin,[3] Zishuo Guo,[1,5] Cong Li,[7] Libiao Zhang,[6,*] Huan Yan,[4,*] Peng Zhou,[2,3,*] Wei Peng,[2,3,*] and Zheng-Li Shi[2,9,*]

[1]Key Laboratory of Virology and Biosafety, Wuhan Institute of Virology, Chinese Academy of Sciences, Wuhan, China
[2]Guangzhou National Laboratory, No. 9 XingDaoHuanBei Road, Guangzhou International Bio Island, Guangzhou, China
[3]The First Affiliated Hospital of Guangzhou Medical University, Guangzhou Medical University, Guangzhou, China
[4]State Key Laboratory of Virology and Biosafety, College of Life Sciences, TaiKang Center for Life and Medical Sciences, Wuhan University, Wuhan, China
[5]University of Chinese Academy of Sciences, Beijing, China
[6]Guangdong Key Laboratory of Animal Conservation and Resource Utilization, Guangdong Public Laboratory of Wild Animal Conservation and Utilization, Institute of Zoology, Guangdong Academy of Sciences, Guangzhou, China
[7]Division of Life Sciences and Medicine, University of Science and Technology of China, Hefei, China
[8]These authors contributed equally
[9]Lead contact
*Correspondence: zhanglb@giz.gd.cn (L.Z.), huanyan@whu.edu.cn (H.Y.), zhou_peng@gzlab.ac.cn (P.Z.), peng_wei@gzlab.ac.cn (W.P.), shi_zhengli@gzlab.ac.cn (Z.-L.S.)
https://doi.org/10.1016/j.cell.2025.01.042

SUMMARY

Merbecoviruses comprise four viral species with remarkable genetic diversity: *MERS-related coronavirus*, *Tylonycteris bat coronavirus HKU4*, *Pipistrellus bat coronavirus HKU5*, and *Hedgehog coronavirus 1*. However, the potential human spillover risk of animal merbecoviruses remains to be investigated. Here, we reported the discovery of HKU5-CoV lineage 2 (HKU5-CoV-2) in bats that efficiently utilize human angiotensin-converting enzyme 2 (ACE2) as a functional receptor and exhibits a broad host tropism. Cryo-EM analysis of HKU5-CoV-2 receptor-binding domain (RBD) and human ACE2 complex revealed an entirely distinct binding mode compared with other ACE2-utilizing merbecoviruses with RBD footprint largely shared with ACE2-using sarbecoviruses and NL63. Structural and functional analyses indicate that HKU5-CoV-2 has a better adaptation to human ACE2 than lineage 1 HKU5-CoV. Authentic HKU5-CoV-2 infected human ACE2-expressing cell lines and human respiratory and enteric organoids. This study reveals a distinct lineage of HKU5-CoVs in bats that efficiently use human ACE2 and underscores their potential zoonotic risk.

INTRODUCTION

Zoonotic spillover is believed to be responsible for the outbreaks of SARS, MERS, and COVID-19.[1–3] Bats harbor the highest proportion of genetically diverse coronaviruses (CoVs) and are considered potential natural reservoirs of the three highly pathogenic human CoVs, SARS-CoV, MERS-CoV, and SARS-CoV-2.[3–8] SARS-CoV and MERS-CoV were documented transmitted to humans via game animals (e.g., civets) or domestic animals (e.g., dromedary camels), whereas the intermediate hosts for SARS-CoV-2 remain unclear.[1,2] Both *in vitro* and *in vivo* studies have demonstrated that bat merbecoviruses, which are phylogenetically related to MERS-CoV, pose a high risk of spillover to humans, either through direct transmission or facilitated by intermediate hosts.[7,9–11] The identification of bat-related merbecoviruses in pangolins (HKU4-CoV) and minks (HKU5-CoV) suggests frequent cross-species transmission of these viruses between bats and other animal species.[12–15]

Receptor recognition and proteolytic activation of the membrane fusion machinery are two critical steps during CoV cell entry, determining the host range and tissue tropism of the viruses. CoV receptor engagement is mediated by receptor-binding domain (RBD) in S1 subunit of their spike (S) glycoprotein, while the membrane fusion between viral and host membranes is promoted by the S2 subunit that activated by the host proteolytic cleavage of S protein.[16] CoVs display promiscuous receptor usage and diverse RBD-binding modes.[17] Dipeptidyl peptidase-4 (DPP4), angiotensin-converting enzyme 2 (ACE2), aminopeptidase N (APN), carcinoembryonic-antigen-related cell adhesion molecule 1 (CEACAM1), and transmembrane serine protease

All rights are reserved, including those for text and data mining, AI training, and similar technologies.

Please cite this article in press as: Chen et al., Bat-infecting merbecovirus HKU5-CoV lineage 2 can use human ACE2 as a cell entry receptor, Cell (2025), https://doi.org/10.1016/j.cell.2025.01.042

2 (TMPRSS2) are five well-known functional protein receptors for CoVs.[18–22] The same receptor usage can be shared by CoVs from different subgenera, as exemplified by the ACE2 receptor usage by human CoV NL63 (subgenus *Setracovirus*) and various SARSr-CoV (subgenus *Sarbecovirus*) with distinct RBD architechtures.[8,19,23] Additionally, CoVs from the same genus, even the same subgenus, may recognize distinct receptors. For instance, unlike SARS-CoV and SARS-CoV-2 using ACE2 as receptor, betacoronaviruses MERS-CoV and MHV recognize receptors DPP4 and CEACAM1, respectively, whereas clade 2 sarbecoviruses were documented to utilize a yet unidentified receptor other than ACE2 for cellular entry.[8,18,19,21,24]

Members of the subgenus *Merbecovirus* also exhibit diverse receptor recognition and binding modes.[25] While DPP4 has been documented as the entry receptor for MERS-CoV, HKU4, and bat MERSr-CoVs (BtCoV-422 and HKU25), several bat MERSr-CoVs, including NeoCoV and MOW15-22, use bat ACE2 orthologs for cell entry and display distinct patterns of multi-species ACE2 tropism.[7,11,18,26–29] During the preparation of this manuscript, two independent teams led by Professors Lekto and Veesler, respectively, released their results that lineage 1 HKU5-CoV (here referred to as HKU5-CoV-1) also use ACE2 orthologs from only a few species including their host, *Pipistrellus abramus* (*P.abr*) bat as receptor.[30,31] However, neither study reported that these HKU5-CoV-1 can efficiently utilize human ACE2 for cellular entry.

In this study, we identified a distinct lineage of merbecovirus HKU5 (lineage 2), here referred to as HKU5-CoV-2, from *Pipistrellus* spp. bats. We demonstrated that bat HKU5-CoV-2 (BtHKU5-CoV-2) efficiently utilized human ACE2 and ACE2 orthologs from various mammalian species for cell entry. Cryoelectron microscopy (cryo-EM) analysis of the complex between BtHKU5-CoV-2 RBD and human ACE2 revealed a binding mode distinct from other known ACE2-using CoVs (e.g., SARS-CoV-2, NL63, NeoCoV, and MOW15-22). Single mutation on most of residues directly participated in BtHKU5-CoV-2 RBD and human ACE2 interaction have limited impact on receptor binding and viral infection. BtHKU5-CoV-2 was successfully isolated from bat sample and confirmed with its ability to infect human ACE2-expressing cells, as well as human respiratory and enteric organoids.

RESULTS

Discovery of a distinct lineage of HKU5-CoV in bats

Bat anal swab samples were screened by pan-CoV PCR targeting the RNA-dependent RNA polymerase (*RdRp*) gene.[4] Five sequences closely related to a previously detected bat HKU5-CoV (sample ID: 141441) we reported in 2021 were identified.[32] The full-length genomic sequences were obtained for all the six HKU5-CoV samples by *de novo* assembly from next-generation sequencing (NGS) data and Sanger sequencing. These bat HKU5-CoVs shared 97.5%–100% similarity to each other and 78.8%–78.9% similarity to HKU5-CoV prototype strain (HKU5-1, GenBank: NC_009020.1) in genomic sequences. According to the latest classification,[33] five conserved replicase domains of these six bat CoVs shared 94.9%–95.1% amino acid identity to HKU5-1, demonstrating that they belong to the species *Pipistrullus* bat CoV HKU5. Further phylogenetic analysis based on complete genome nucleotide sequences and amino acid sequences of S protein revealed that these six HKU5-CoVs form a distinct lineage (lineage 2, hereafter referred to as HKU5-CoV-2) from all previous reported HKU5-CoVs, which belong to lineage 1 (hereafter referred to as HKU5-CoV-1) (Figures 1A and 1B). Bat HKU5-CoV-2 141441 (BtHKU5-CoV-2-441) was selected as a representative strain of this distinct lineage for further analysis. Similarity plot analysis indicated that the BtHKU5-CoV-2-441 exhibits the highest identity with other five BtHKU5-CoV-2 strains throughout the entire genome among merbecoviruses, with BtHKU5-CoV-2-153 and BtHKU5-CoV-2-155 showing reduced identity in the *S* genes (Figures 1C and S1A). Comparison of amino acid sequences of individual proteins also showed high similarity between BtHKU5-CoV-2-441 and other five BtHKU5-CoV-2. The S1 protein of BtHKU5-CoV-2-441 shared 91.2%–99.2% amino acid similarity with other BtHKU5-CoV-2, but very low (57.4%) similarity with HKU5-CoV-1 (Figure 1D; Table S1). Consistently, analysis of regions corresponding to MERS-CoV RBD revealed that BtHKU5-CoV-2 shared only 56.1%–57% amino acid sequence similarity with HKU5-CoV-1 and much lower (31.8%–55.4%) similarity with other merbecoviruses, except for HKU25-CoV (59.3%–62.8%), suggesting a distinct receptor usage or binding mode of BtHKU5-CoV-2 from other merbecoviruses (Figures S1B and S1C).

Bat lineage 2 HKU5-CoV utilize human ACE2 as receptor

Previous studies showed that multiple merbecoviruses identified in bats pose a potential risk for human emergence, as they efficiently utilize human DPP4 for cell entry and caused interstitial pneumonia in human DPP4 transgenic mice.[9,10] We first tested the susceptibility of human cell lines using the BtHKU5-CoV-2-441 S pseudotyped vesicular stomatitis virus (VSV) and found that Caco-2 and Huh7.5.1 cells, but not HEK293 cells, permitted the pseudotyped virus entry with trypsin treatment (Figure S2A). To evaluate whether BtHKU5-CoV-2 can utilize the four known CoV receptors-human ACE2, DPP4, APN, or CEACAM1, we prepared VSV-pseudotyped viruses carrying the BtHKU5-CoV-2-441 S protein, using pseudotyed virus carrying MERS-CoV-S, SARS-CoV-S, or HKU5-CoV-1 S protein as controls. We found that HEK293 cells overexpressing human ACE2 supported efficient BtHKU5-CoV-2-441 pseudotyped virus entry with trypsin treatment (Figures 2A–2D). As expected, pseudotyped viruses carrying MERS-CoV-S showed efficient entry in HEK293 cells overexpressing human DPP4, while pseudotyped virus carrying the SARS-CoV-S efficiently entered HEK293 cells overexpressing the human ACE2. However, no or very limited entry was observed for the HKU5-CoV-1 pseudotyped virus in the cells overexpressing any of the four known CoV receptors. Notably, BtHKU5-CoV-2-441 entry was almost abolished in ACE2 knockout Huh-7 cells, which can be restored upon human ACE2 overexpression (Figure 2E). Consistently, a dual split protein-based fusion assay demonstrated that human ACE2 promoted efficient cell-cell fusion in the presence of BtHKU5-CoV-2-441 S protein, but not with the HKU5-CoV-1 S protein (Figures 2F–2H). Taken together, these results indicate that BtHKU5-CoV-2 can use human ACE2 as a functional receptor for cell entry.

Please cite this article in press as: Chen et al., Bat-infecting merbecovirus HKU5-CoV lineage 2 can use human ACE2 as a cell entry receptor, Cell (2025), https://doi.org/10.1016/j.cell.2025.01.042

CellPress

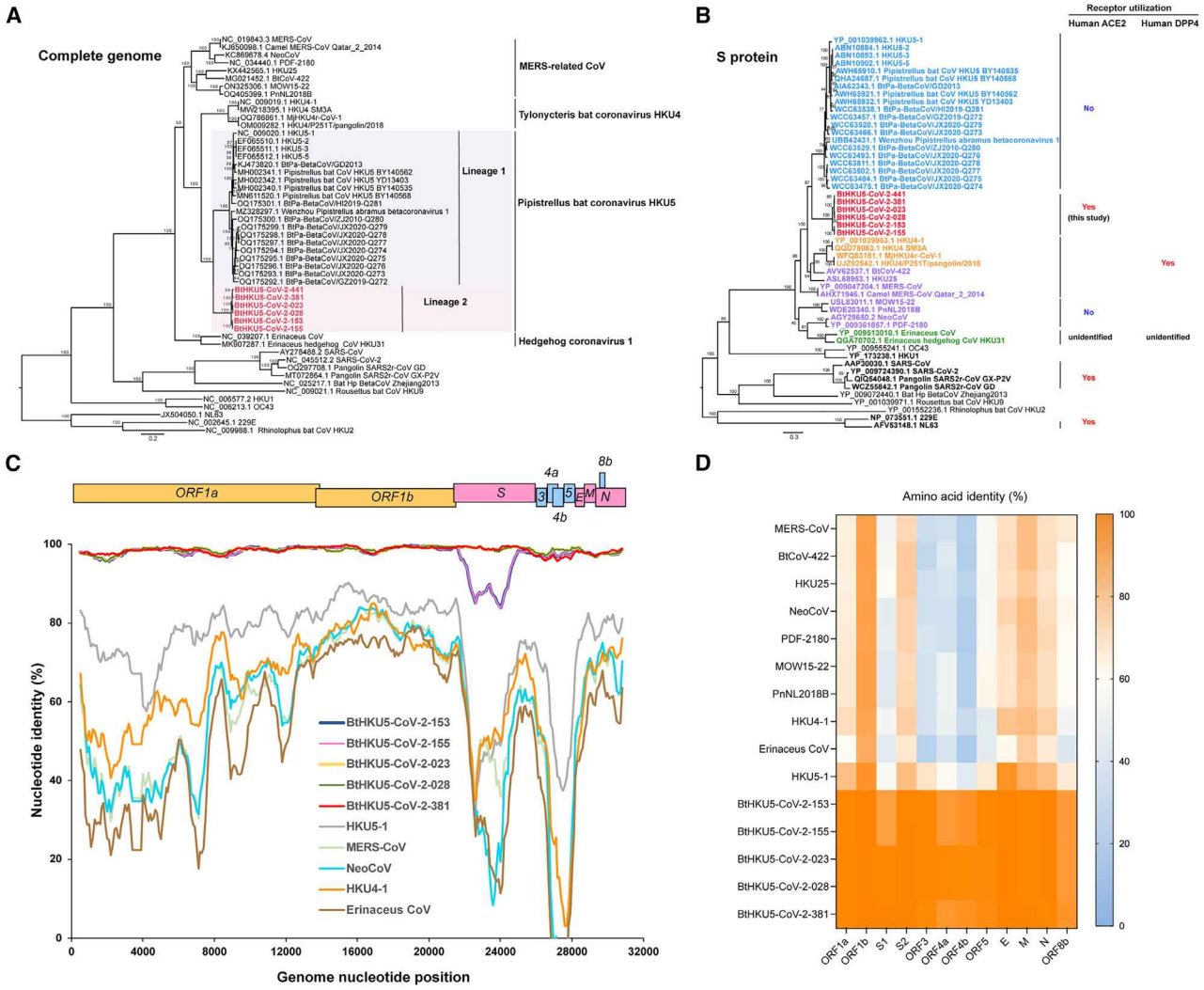

Figure 1. Genome characteristics of bat lineage 2 HKU5-CoVs

(A) Phylogenetic tree based on the complete genomic sequences of representative coronaviruses. The scale bar represents 0.2 substitutions per nucleotide position.

(B) Phylogenetic analysis of representative coronaviruses using spike protein amino acid sequences. Human receptor information is indicated at the right of the tree. The scale bar represents 0.3 substitutions per amino acid position.

(C) Similarity plot analysis of HKU5-CoV-2 and representative merbecoviruses, based on the full-length genome sequences. BtHKU5-CoV-2-441 was used as the query sequence. BtHKU5-CoV-2-153 and BtHKU5-CoV-2-023 are bolded.

(D) Heatmap of amino acid identities of individual viral proteins of representative merbecoviruses compared with those of BtHKU5-CoV-2-441. Spike protein has been divided into two functional subunits, S1 and S2.

See also Figure S1 and Table S1.

To assess the potential host range of BtHKU5-CoV-2, we examined the receptor function of 54 ACE2 orthologs from nonhuman primates, other mammals and birds. Most mammalian and avian ACE2 orthologs supported efficient entry of BtHKU5-CoV-2-441 pseudotyped viruses, suggesting a potentially broad host range of BtHKU5-CoV-2 (Figures 2I and S2B). We also screened an ACE2 library comprising 57 bat ACE2 orthologs using BtHKU5-CoV-2-441 pseudotyped viruses and RBD proteins. BtHKU5-CoV-2-441 pseudotyped viruses showed efficient entry in cells expressing multiple Yinpterochiropteran and Yangochiropteran bat ACE2 orthologs (Figures 2J and S2C). In line with these findings, BtHKU5-CoV-2-441 RBD showed broad-spectrum binding to various bat ACE2 orthologs, but resistant to *P.abr* ACE2 from the host of BtHKU5-CoV-1 (Figure S2D). Collectively, these results indicate that BtHKU5-CoV-2-441 exhibits a potentially broad host tropism in terms of ACE2 receptor usage.

Structural basis for human ACE2 usage by BtHKU5-CoV-2-441

Surface plasmon resonance (SPR) assays were conducted to evaluate the binding affinity between the RBD of BtHKU5-CoV-2-441 and human ACE2. The results demonstrated that the

Please cite this article in press as: Chen et al., Bat-infecting merbecovirus HKU5-CoV lineage 2 can use human ACE2 as a cell entry receptor, Cell (2025), https://doi.org/10.1016/j.cell.2025.01.042

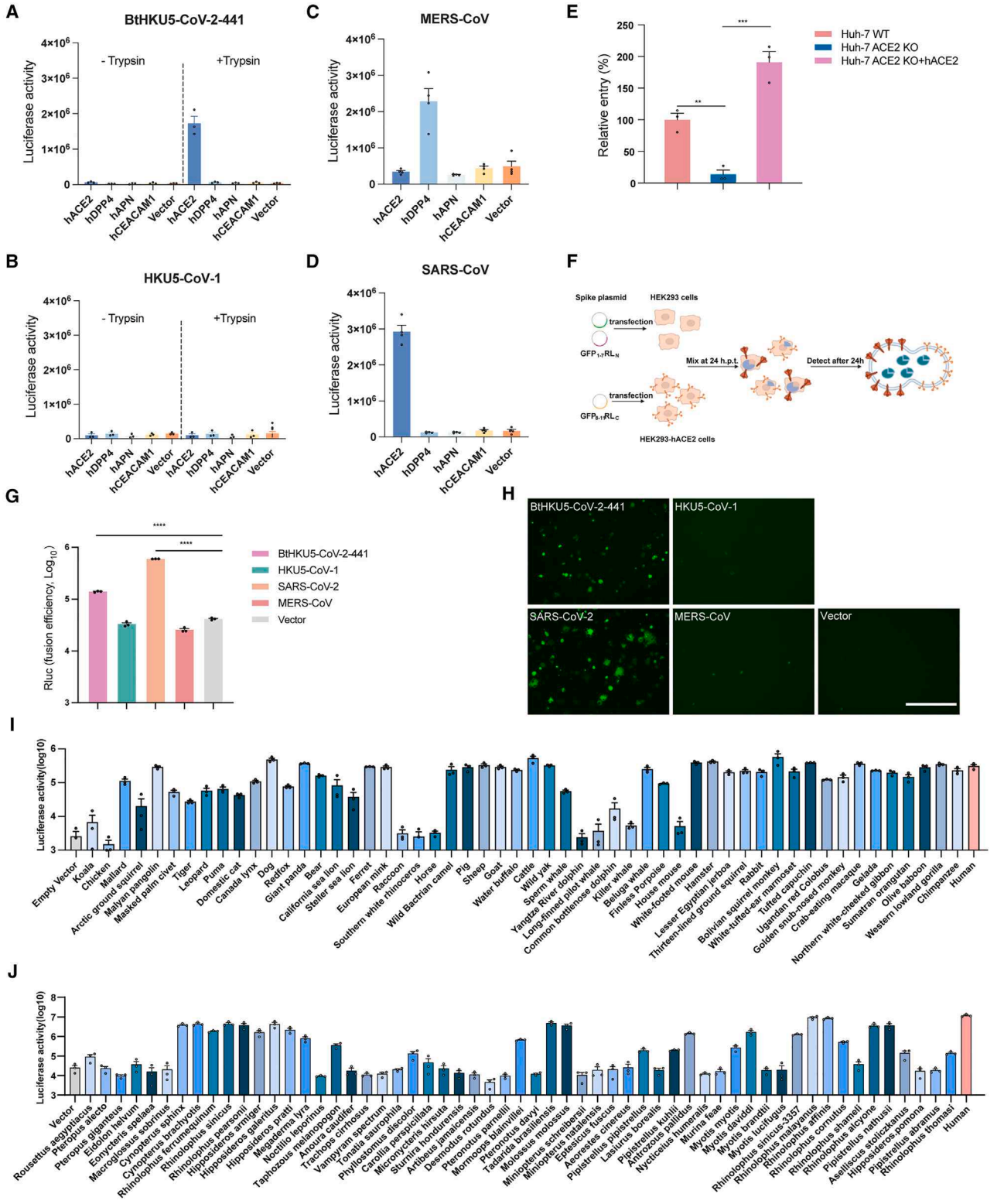

Figure 2. BtHKU5-CoV-2-441 utilizes human ACE2 as a functional receptor for cell entry

(A–D) Receptor usage for BtHKU5-CoV-2-441 pseudotyped virus entry. Entry of pseudotyped viruses harboring BtHKU5-CoV-2-441 (A), HKU5-CoV-1(B), MERS-CoV (C), and SARS-CoV (D) S were transduced into the HEK293 cells transiently expressing human ACE2 (hACE2), human DPP4 (hDPP4), human APN

(legend continued on next page)

Please cite this article in press as: Chen et al., Bat-infecting merbecovirus HKU5-CoV lineage 2 can use human ACE2 as a cell entry receptor, Cell (2025), https://doi.org/10.1016/j.cell.2025.01.042

BtHKU5-CoV-2-441 RBD binds effectively to human ACE2, with an affinity of 6.55 × 10^{-6} M (Figure 3A). The cryo-EM single particle structure of the BtHKU5-CoV-2-441 RBD-hACE2 complex were resolved at 2.96 Å (Figure S3A; Table S2). 3D reconstruction results revealed that the four-stranded anti-parallel β-sheet (β6-β9) of the BtHKU5-CoV-2-441 RBD interacts with the α1, α10, α11, and β5 regions of human ACE2, mediated by a network of polar and hydrophobic interactions. The interaction surface between the BtHKU5-CoV-2-441 RBD and human ACE2 can be roughly divided into two distinct patches, patch 1 and patch 2. In patch 1, residues R504, R496, A500 (main chain O atom), and S524 of RBD interact with H34, E37, Q96, and A387 of human ACE2 via potential polar contacts. In patch 2, Y448, S453, R493, and D537 of the RBD interact with Y41, N330, Q325, and K353 of human ACE2 through polar contacts (Figures 3B, 3C, and S3B; Table S3). Analysis of hydrophobic interactions revealed a small portion of human ACE2 hydrophobic surface participates in the interaction with BtHKU5-CoV-2-441 RBD. Specifically, residues such as L494, A500, F501, Y533, and V535 interact with the hydrophobic regions of human ACE2 (Figure S3C). Glycosylation modification seems do not play a significant role in the interaction between human ACE2 and BtHKU5-CoV-2-441 RBD.

Unlike SARS-CoV-2, the merbecoviruses BtHKU5-CoV-2-441, MERS-CoV, HKU4-CoV, HKU5-CoV-1, and NeoCoV RBDs share similar core subdomain structures and all carry four-stranded anti-parallel (β6-β9) β-sheets as their receptor-binding motifs, with the loops connecting β6-β9 showing different length and conformations (Figures S3D and S3E). A comparative analysis of the RBD-binding footprint of BtHKU5-CoV-2-441, NeoCoV,[27] SARS-CoV-2,[34] SARS-CoV,[35] and NL63[36] on ACE2 indicate the BtHKU5-CoV-2-441 RBD largely overlaps with SARS-CoV, SARS-CoV-2, and NL63 RBD footprints, while sharing minimal overlap with that of NeoCoV (Figure 3D). Notably, the residues N330 and E329 are frequently involved in the interactions across all these ACE2-binding RBDs. Residues N90, T92, and Q96 are specific for BtHKU5-CoV-2 receptor recognition, while residues A386, A387, Q388, and P389 of human ACE2 are used by BtHKU5-CoV-2 and NL63 but not by SARS-CoV or SARS-CoV-2 (Figure 3E). Structural superimposition further demonstrate that BtHKU5-CoV-2-441 utilizes a distinct binding mode to engage human ACE2 from other ACE2-binding CoVs (Figure 3F).

Determinants of human ACE2 recognition

To characterize the determinants of human ACE2 recognition by the BtHKU5-CoV-2-441 RBD, structure guided mutagenesis analysis was conducted. SPR experiments revealed that single-point mutations (Y448A, R504A, S524A, and D537A) involved in the interaction surface in the BtHKU5-CoV-2-441 RBD led to a slight reduction in binding affinity and pseudotyped virus entry in HEK293-hACE2 cells (Figures 4A and 4B). However, multiple-site mutations involving both hydrophilic and hydrophobic interactions in BtHKU5-CoV-2-441 RBD had a pronounced effect on binding affinity with human ACE2 (Figure 4A). Consistent with this, pseudotyped virus entry efficiency was hampered sharply by these multiple-site mutations (Figure 4B). To further explore the binding determinants on human ACE2, we substituted the corresponding residues in the non-functional ACE2 orthologs from three bat species, *Sturnira hondurensis* (*S.hon*), *Pipistrellus pipistrellus* (*P.pip*), and *Lasiurus borealis* (*L.bor*), with those of human ACE2. The E353K mutation in *P.pip* ACE2 and K30D mutation in *L.bor* ACE2 notably enhanced RBD-binding ability and pseudotyped virus entry efficiency. Similarly, the DVK90-92NLT mutation, as well as the double mutation DVK90-92NLT/N384A in *S.hon* ACE2, enhanced the ability of the ortholog to promote pseudotyped virus entry, despite no apparent increase in RBD binding (Figures 4C and 4D). Conversely, except for the E37K mutation, all other tested single substitutions in human ACE2 that disrupted hydrogen bonds or salt bridges had little effect on RBD binding or pseudotyped virus entry (Figures 4E and 4F). Double mutations E37K/D30A and E37K/H34G further decreased human ACE2 usage efficiency of BtHKU5-CoV-2-441. In contrast, the double mutation E329G/N330G and the multiple mutation T92I/T324G/Q325G had minimal impact on RBD binding and pseudotyped virus entry (Figure S4). All of these data demonstrated that E37 is a critical residue for human ACE2 engagement by BtHKU5-CoV-2-441 and highlighted the well adaptation of BtHKU5-CoV-2-441 to human ACE2.

Isolation and infection of bat lineage 2 HKU5-CoV in ACE2-expressing cells

One BtHKU5-CoV-2 strain was successfully isolated from a bat anal swab sample (ID: 223023, here named as BtHKU5-CoV-2-023). NGS confirmed that the genomic sequence of the cultured virus matched the original BtHKU5-CoV-2-023 sequence (Figure S5). Cytopathogenic effects (CPEs), positive immunofluorescence staining for nucleocapsid protein (NP), and an increase in viral load were observed following BtHKU5-CoV-2-023 infection in Caco-2-hACE2 cells (Figures 5A and 5B). The expression of human ACE2, but not human DPP4, APN, or CEACAM1, efficiently supported BtHKU5-CoV-2-023 infection in HEK293 cells (Figure 5C). Susceptibility to BtHKU5-CoV-2-023 infection was

(hAPN), human CEACAM1 (hCEACAM1). Empty vector was used as a negative control. The entry efficiency of BtHKU5-CoV-2-441 and HKU5-CoV-1 pseudotyped viruses was also assessed under trypsin treatment (0.5 μg/mL).

(E) Entry efficiency of BtHKU5-CoV-2-441 pseudotyped viruses in wild-type Huh-7, ACE2 knockout Huh-7 (Huh-7 ACE2 KO), and Huh-7 ACE2 KO cells transiently transfected with human ACE2 expression plasmid. Pseudotyped viruses were transduced under 0.5 μg/mL trypsin treatment.

(F–H) Analysis of BtHKU5-CoV-2-441 and HKU5-CoV-1 S-protein-mediated cell-cell fusion in HEK293 cells expressing human ACE2 without trypsin. SARS-CoV-2 and MERS-CoV S proteins serve as positive and negative controls, respectively. The schematic model of cell-cell fusion assay is shown (F). Fusion efficiencies are presented as *Renilla* luciferase activity (G) and GFP intensity (H), respectively. Scale bars: 400 μm.

(I and J) Receptor function of ACE2 orthologs from non-bat mammals and birds (I) and bats (J) for BtHKU5-CoV-2-441. Entry efficiency of pseudotyped viruses in HEK293 or HEK293T cells transiently expressing the known CoV receptors and ACE2 orthologs was determined by firefly luciferase activity. Pseudotyped viruses were transduced with trypsin treatment. For (J), pseudoviruses were pretreated with 100 μg/mL TPCK-trypsin.

Data are presented as means and SEMs of at least triplicate measurements in (A)–(E), (G), (I), and (J). Statistical significance was assessed using a two-tailed Student's t test. See also Figure S2.

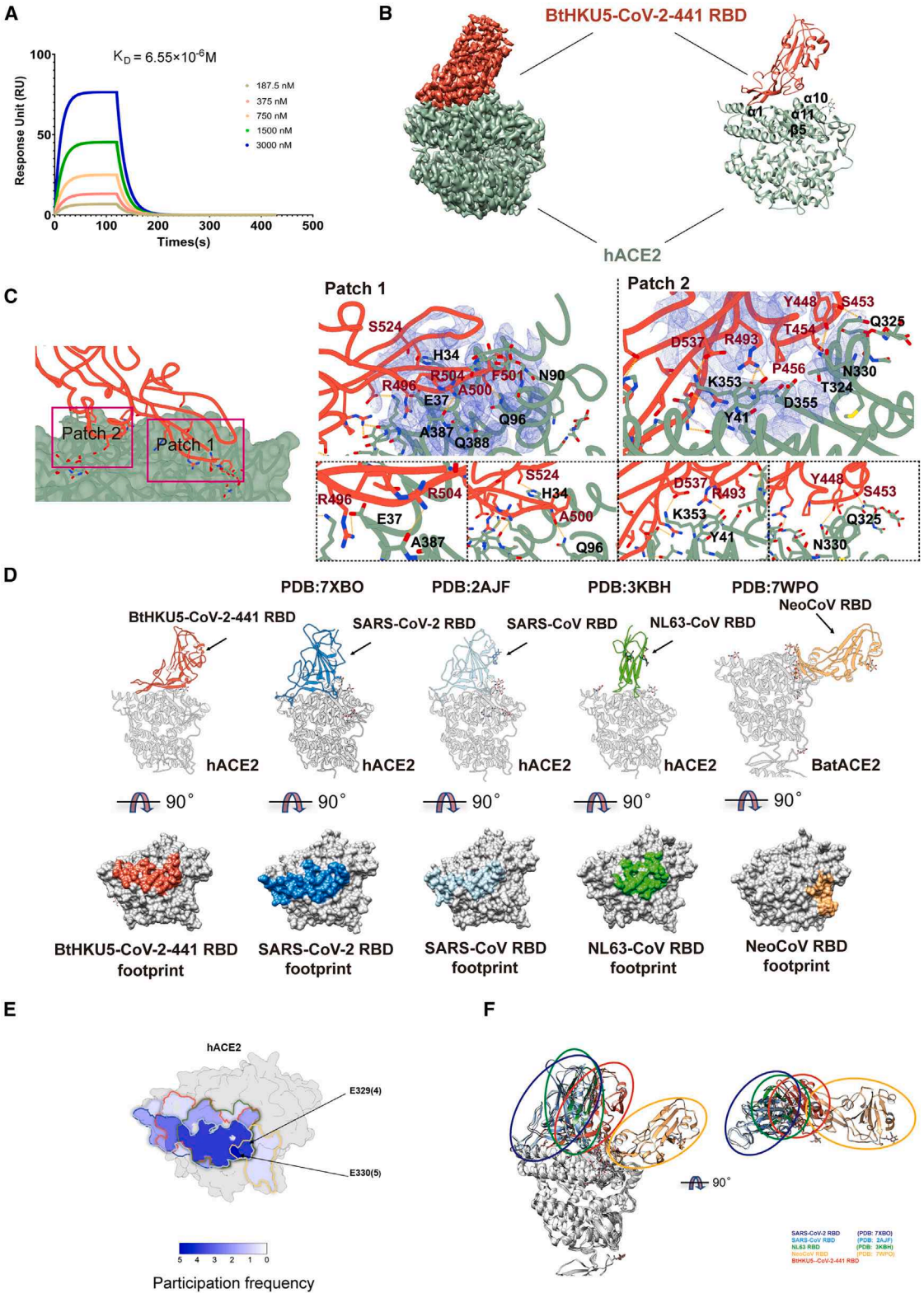

Figure 3. Cryo-EM structure analysis of BtHKU5-CoV-2-441 RBD in complex with human ACE2

(A) SPR analyses of binding kinetics of the human ACE2 ectodomains to BtHKU5-CoV-2-441 RBD immobilized on CM5 biosensors.

(B) Cryo-EM structure of BtHKU5-CoV-2-441 RBD bound to human ACE2. The electron map (left) and ribbon representation (right) are shown.

(legend continued on next page)

Please cite this article in press as: Chen et al., Bat-infecting merbecovirus HKU5-CoV lineage 2 can use human ACE2 as a cell entry receptor, Cell (2025), https://doi.org/10.1016/j.cell.2025.01.042

abolished by human ACE2 knockout and restored by human ACE2 overexpression in Huh-7 ACE2 KO cells and Caco-2 ACE2 KO cells. Overall, BtHKU5-CoV-2-023 amplified more efficiently in Caco-2 cells than in Huh-7 cells (Figures 5D and 5E). The infection of BtHKU5-CoV-2-023 could be blocked by ACE2-targeting antibody h11B11,[37] as well as SARS-CoV-2 and SARS-CoV RBD proteins, but not MERS-CoV RBD protein (Figures 5F and 5G). The susceptibility of HEK293 to BtHKU5-CoV-2-023 can be significantly enhanced by the exogenous expression of pangolin ACE2. A lesser extent of improvement is observed with *Pipistrellus kuhlii* (P. kuh) ACE2 expression, but there is no effect when using *P.abr* ACE2 (Figure 5H). These results further confirmed that ACE2 served as the functional receptor for bat lineage 2 HKU5-CoV infection.

Inhibition of cell entry and replication of bat lineage 2 HKU5-CoVs

MERS-CoV relies on serine protease TMPRSS2 and endosomal cysteine protease cathepsin L for S protein proteolytic activation and viral entry.[38] To assess the protease dependency of lineage 2 HKU5-CoVs, we evaluated BtHKU5-CoV-2-441 entry efficiency under treatment of protease inhibitors. We observed that the entry efficiency of BtHKU5-CoV-2-441 pseudotyped viruses was suppressed upon treatment of cysteine-class proteases inhibitor E64d, serine-class transmembrane proteins inhibitor camostat, furin inhibitor decanoyl-Arg-Val-Lys-Arg chloromethyl ketone (decRVKRcmk), endosomal acidification inhibitor bafilomycin A1 (BafA1) and hydroxychloroquine, as well as knockdown of cathepthin L and furin, in Caco-2-hACE2 cells. BtHKU5-CoV-2-023 infection in Caco-2-hACE2 cells was also suppressed by camostat or E64D treatment, and more efficiently by their combination. These results demonstrated that BtHKU5-CoV-2 can employ both TMPRSS2 and cathepsin L for S protein proteolytic activation (Figures S6A–S6D). Similar to MERS-CoV and SARS-CoV-2, the BtHKU5-CoV-2-441 S protein contains an S1/S2 furin cleavage site (RGSR). Consequently, S proteolytic cleavage during biogenesis can be detected in BtHKU5-CoV-2-441 S pseudotyped viruses, although this process occurs less efficiently than in MERS-CoV. Additionally, the cleavage of S from both viruses can be enhanced by furin overexpression (Figures S6E and S6F). In order to address the role of S1/S2 and S2′ cleavage sites, respectively, we generated S protein mutants with the first arginine residues replaced with alanine residues. While the S proteolytic processing is more affected by the S1/S2 site mutation, cell-cell fusion mediated by BtHKU5-CoV-2-441 S protein was more significantly impaired by mutation in S2′ cleavage site. These results demonstrate that the processing of both the S1/S2 and S2′ cleavage sites contribute to cell-cell fusion, with cleavage at the S2′ site playing a more critical role in this process (Figures S6G–S6J).

As the respiratory and enteric track is the primary target organ of human CoVs for infection, we tested the ability of BtHKU5-CoV-2-023 propagate in human respiratory and enteric organoids.[8,39,40] The virus replicated in these organoids, with viral loads increasing by 1.5 to 2 log units, suggesting that BtHKU5-CoV-2-023 has the potential to propagate in the human respiratory and enteric track (Figures S6K–S6M). We then explored potential therapeutic countermeasures against BtHKU5-CoV-2, including human-derived monoclonal antibodies targeting the MERS-CoV RBD (m336),[41] the SARS-CoV-2 RBD (REGN10933 and REGN10987),[42] the CoV S2 subunit (76E1 and S2P6),[43,44] and the CoV fusion inhibitor (EK1C4).[45] While m336, REGN10933, and REGN10987 showed no neutralizing activity, 76E1, S2P6, and EK1C4 peptide efficiently suppressed BtHKU5-CoV-2-441 pseudotyped virus entry (Figures 6A–6F). Subsequently, we demonstrated the potent antiviral potency of three small molecules, nirmatrelvir, remdesivir, and GC376, which have been demonstrated broad-spectrum inhibition against CoVs[46–48] (Figures 6G–6I).

DISCUSSION

HKU5-CoV was first detected in bats in 2006 and is prevalent in *Pipistrellus abramus* bats in eastern and southern Asia.[32,49–52] These viruses remained poorly characterized until two recent preprints posted during the preparation of our manuscript, reported the utilization of bat ACE2 by lineage 1 HKU5-CoV and described the complex structure between the RBD and *Pipistrellus abramus* bat ACE2. In this study, we report the discovery and isolation of a distinct lineage (lineage 2) of HKU5-CoV, which can utilize not only bat ACE2 but also human ACE2 and various mammalian ACE2 orthologs. Our data suggest that BtHKU5-CoV-2 exhibits better adaptation to human ACE2 compared with HKU5-CoV-1, as evidenced by enhanced binding affinity, tolerated point mutation on interacting residues, increased infection efficiency in human cells, and replication in human cells and organoids. These results indicate that the HKU5-CoV-2 may have a broader host range and a higher potential for interspecies infection. Notably, viral sequences closely related to bat HKU5-CoV were recently detected in farmed minks, providing evidence of interspecies transmission of HKU5-CoV in nature.[15] Our results underscore the importance of enhanced surveillances and further research on HKU5-CoVs to better understand their zoonotic potential and interspecies transmission dynamics.

Complex receptor engagement revealed that betacoronaviruses can be grouped based on their receptor usage into DPP4-utilizing, ACE2 utilizing, and those with unidentified

(C) Close-up view of BtHKU5-CoV-2-441 RBD-hACE2 interaction interface consists of two different patches. The residues participated in polar interaction are shown. The hydrogen bonds are indicated by yellow dash lines.
(D) RBD-binding structures and receptor (human ACE2 for BtHKU5-CoV-2-441, SARS-CoV-2, SARS-CoV, NL63, and Bat ACE2 for NeoCoV) footprints of indicated ACE2-using sarbecoviruses and merbecoviruses.
(E) Overlay of RBD footprints on ACE2. The heatmap indicates the per-residue frequency of participation in virus-ACE2 interfaces. Residues 329–330 are identified as a virus-binding hotspots.
(F) Comparison of receptor-binding modes among ACE2-using coronaviruses.
See also Figure S3 and Tables S2 and S3.

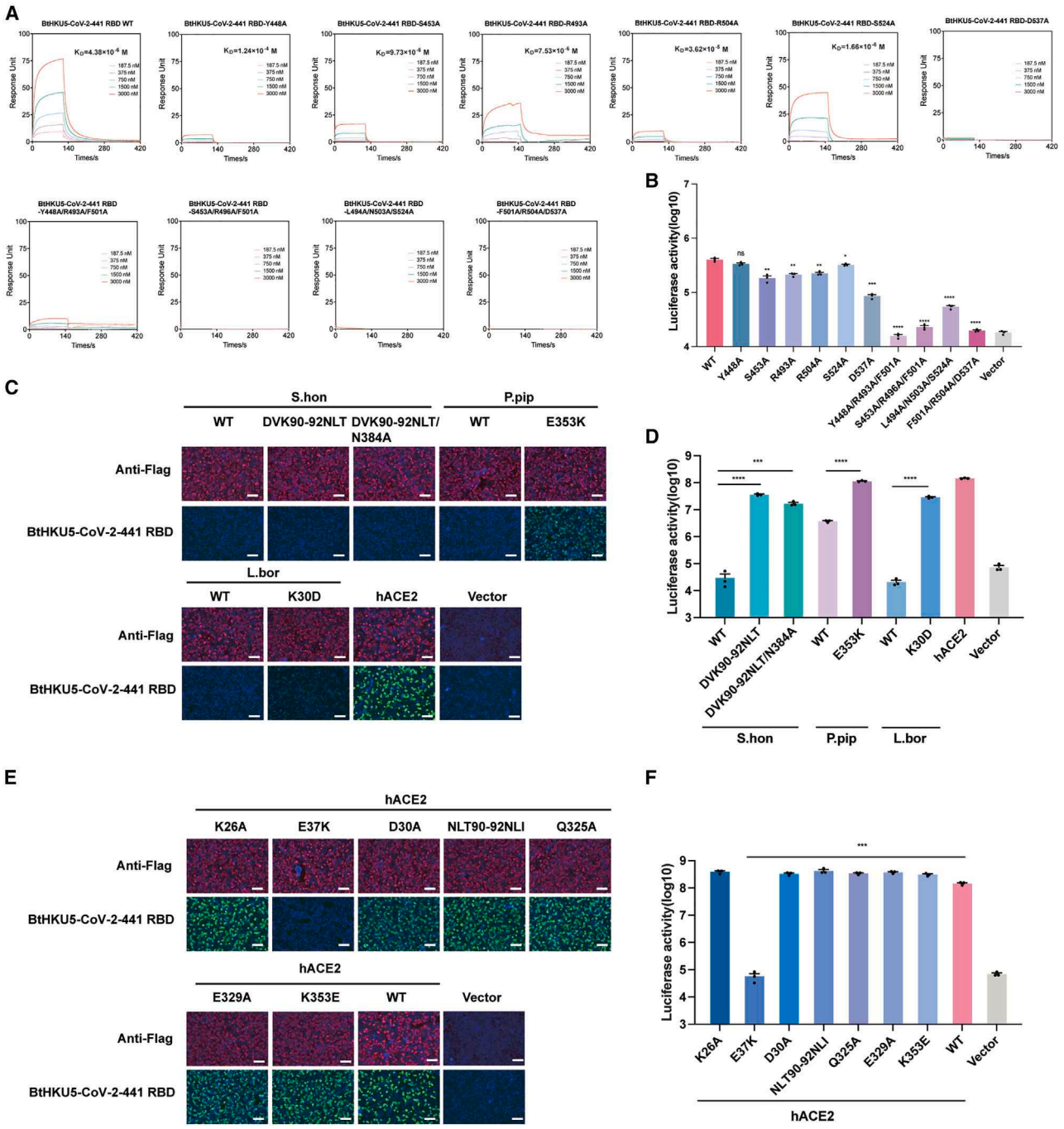

Figure 4. Molecular determinants of ACE2 recognition by BtHKU5-CoV-2-441

(A) SPR analyses of binding kinetics of the human ACE2 ectodomains to wild-type and mutant BtHKU5-CoV-2-441 RBD immobilized on CM5 biosensors.

(B) Entry efficiency of pseudotyped viruses packaged with wild-type and mutant BtHKU5-CoV-2-441 S proteins in HEK293-hACE2 cells. Pseudotyped viruses were transduced with trypsin treatment.

(C and D) The RBD binding (C) and pseudtyped virus entry (D) efficiency promoted by *S.hon*, *P.pip*, and *L.bor* ACE2 orthologs harboring indicated mutations corresponding to human ACE2 equivalent residues.

(E and F) Impact of indicated human ACE2 mutations on BtHKU5-CoV-2-441 RBD binding and pseudotyped virus entry (F) efficiency. Pseudotyped viruses were transduced with trypsin treatment.

In (C) and (E), scale bars, 100 μm; RBD binding in green; nuclei in blue. Data are presented as means and SEMs of $n = 3$ biological replicates in (B), (D), and (F). Statistical significance was assessed using a two-tailed Student's t test. In (B), all mutant columns are compared with wild-type column, respectively. See also Figure S4.

Please cite this article in press as: Chen et al., Bat-infecting merbecovirus HKU5-CoV lineage 2 can use human ACE2 as a cell entry receptor, Cell (2025), https://doi.org/10.1016/j.cell.2025.01.042

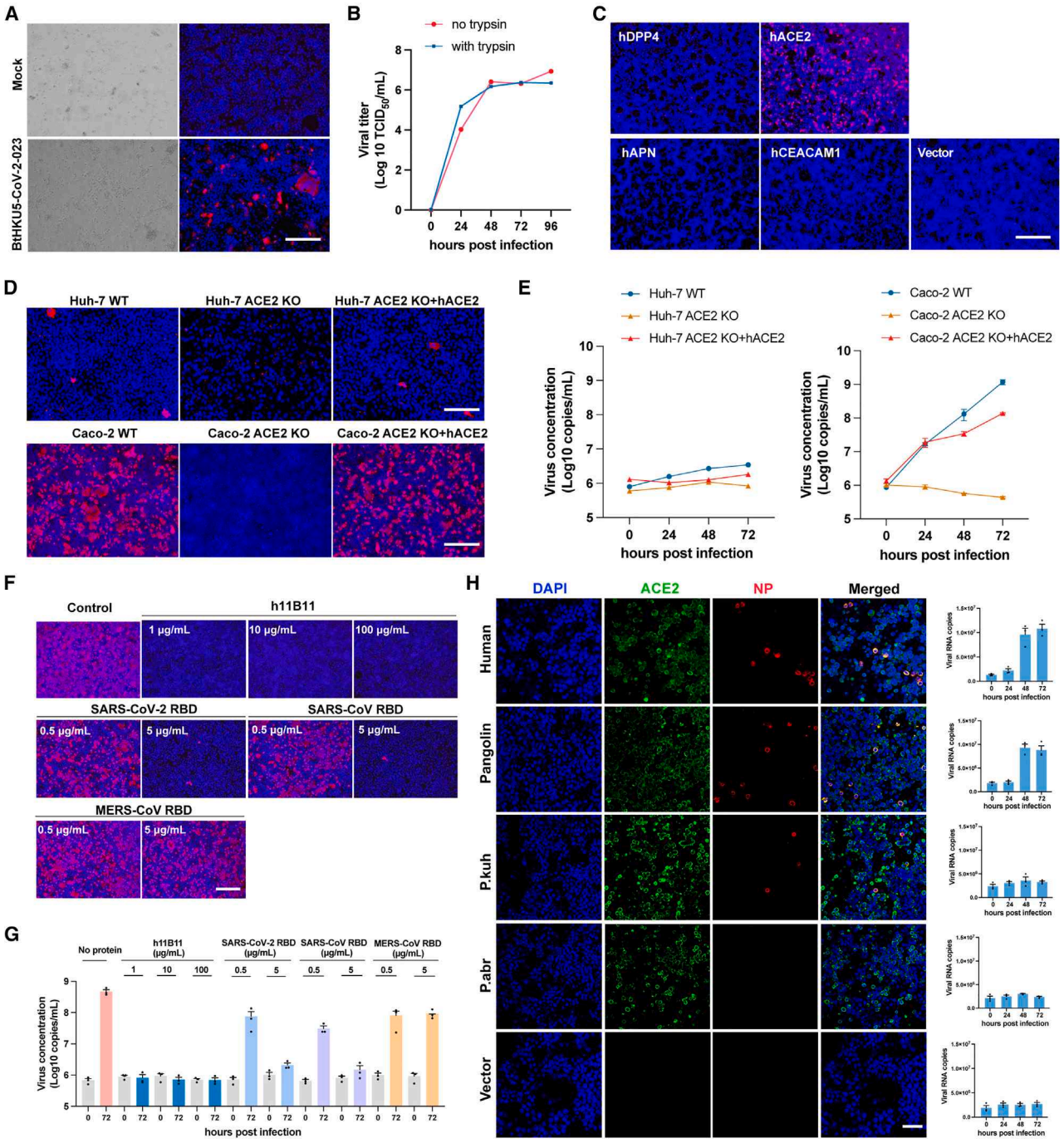

Figure 5. Isolation and infection of bat lineage 2 HKU5-CoV in cells expressing ACE2

(A) Cytopathic effects (left) in Caco-2-hACE2 cells infected with BtHKU5-CoV-2-023 or mock infected at 5 d.p.i., and immunofluorescence assay (IFA) analysis of the infection with an antibody against the BtHKU5-CoV-2-441 NP (right).

(B) Caco-2-hACE2 cells were infected with BtHKU5-CoV-2-023 at a multiplicity of infection (MOI) of 0.05 with or without trypsin (5 μg/mL treatment). Viral titers at the indicated time points were determined by 50% tissue culture infectious dose ($TCID_{50}$) assay.

(C) HEK293 cells transiently expressing human ACE2 (hACE2), human DPP4 (hDPP4), human APN (hAPN), human CEACAM1 (hCEACAM1), or empty vector were infected with BtHKU5-CoV-2-023 at an MOI of 0.2 and detected by IFA at 72 h.p.i .

(D and E) Wild-type and human ACE2 knockout Huh-7/Caco-2 (Huh-7 ACE2 KO/Caco-2 ACE2 KO) cells, as well as human ACE2 expression restored Huh-7 ACE2 KO/Caco-2 ACE2 KO cells were infected with BtHKU5-CoV-2-023 at an MOI of 0.01 for 72 h, and viral infection was analyzed by IFA (D) and quantitative reverse transcription PCR (qRT-PCR) (E).

(legend continued on next page)

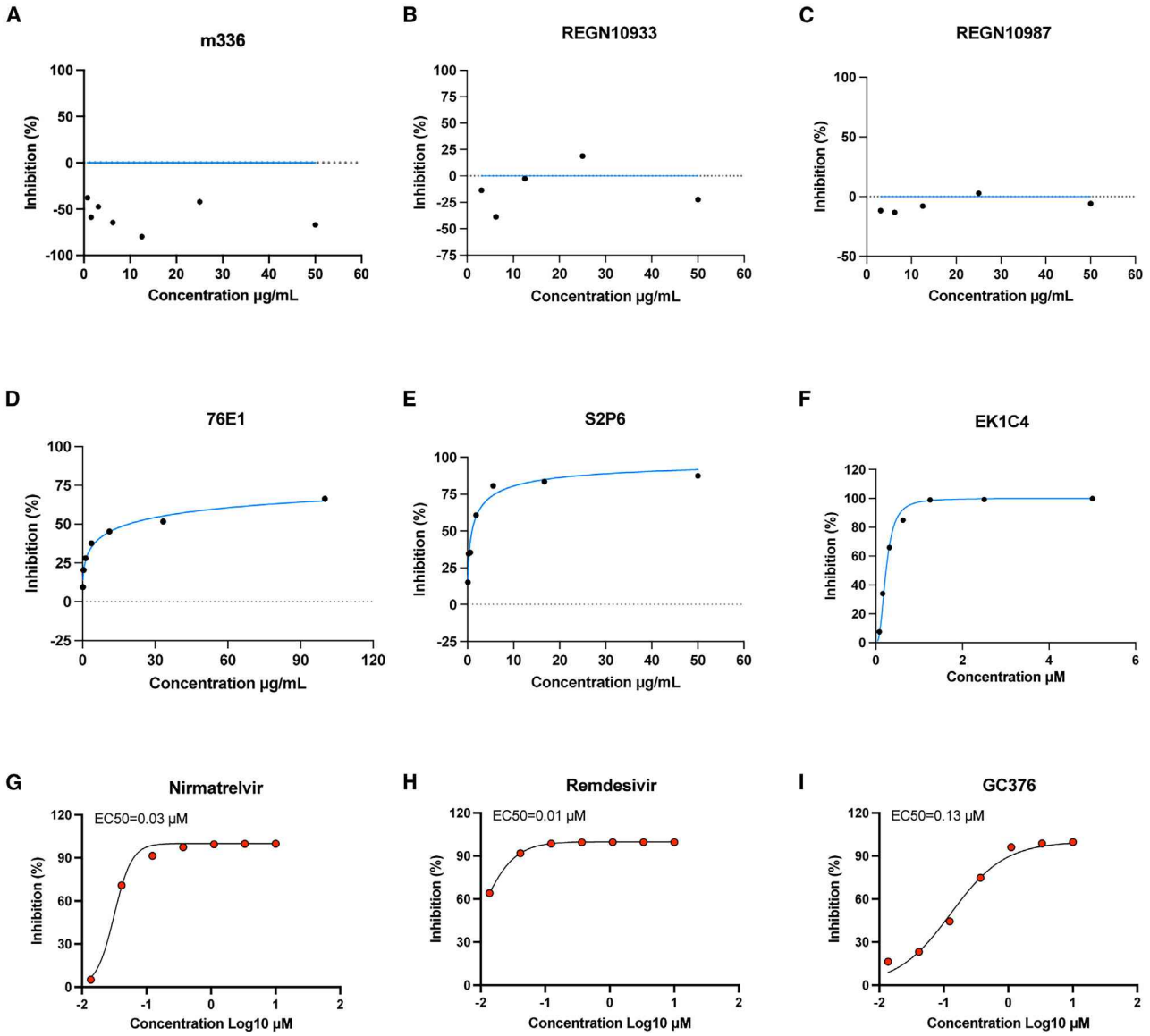

Figure 6. Inhibition of cell entry and replication of bat lineage 2 HKU5-CoV

(A–F) Neutralization or inhibition efficacy of human monoclonal antibodies targeting the MERS-CoV RBD (A), the SARS-CoV-2 RBD (B and C), SARS-CoV-2 S2 (D and E), or broad-spectrum coronavirus fusion peptide inhibitor (F) against BtHKU5-CoV-2-441, as quantified by cell entry efficiency of BtHKU5-CoV-2-441 pseudotyped virus. BtHKU5-CoV-2-441 pseudotyped virus transduced Caco-2-hACE2 cells without trypsin treatment.

(G–I) Antiviral activities of small molecules nirmatrelvir (G), remdesivir (H), and GC376 (I) against BtHKU5-CoV-2-023 authentic virus, as determined by qRT-PCR. Data are presented as means and SEMs of at least duplicate measurements. See also Figure S6.

receptors. The DPP4-utilizing CoVs include MERS-CoV, certain bat MERSr-CoVs (BtCoV-422 and HKU25) and pangolin and bat HKU4-CoVs, all of which utilize human DPP4 in addition to their natural host receptors.[7,9,11,26] The ACE2-utilizing CoVs include SARS-CoV-1/2, various bat and pangolin SARSr-CoVs, some bat MERSr-CoVs (NeoCoV and MOW15-22) and

(F and G) Caco-2-hACE2 cells were pretreated with antibody, RBD proteins or mock-treated at 37°C for 2 h and infected with BtHKU5-CoV-2-023 at an MOI of 0.01 for 72 h. Viral infection was analyzed by IFA (F) and qRT-PCR (G).

(H) HEK293 cells overexpressing the indicated ACE2 orthologs were infected with BtHKU5-CoV-2-023 at an MOI of 0.01 and detected by IFA at 72 h.p.i. (red, NP; green, ACE2; blue, nuclei; scale bars, 50 μm) and qRT-PCR.

In (A), (C), (D), and (F), scale bars, 300 μm; red, NP; blue, nuclei. Data are presented as means and SEMs of at least triplicate measurements in (B), (E), (G), and (H). See also Figure S5.

Please cite this article in press as: Chen et al., Bat-infecting merbecovirus HKU5-CoV lineage 2 can use human ACE2 as a cell entry receptor, Cell (2025), https://doi.org/10.1016/j.cell.2025.01.042

HKU5-CoV.[3,8,19,27,28,53–55] In addition to betacoronavirus, the alphacoronavirus HCoV-NL63 also utilizes ACE2, suggesting that the receptor switch may have occurred during virus transmission between bat families, genera, or species.[23] Interestingly, these ACE2-utilizing CoVs exhibit distinct receptor recognition modes. For example, NeoCoV and MOW15-22, which recognize only bat ACE2, have a different binding model compared with SARS-CoV-2 and NL63 RBD-hACE2.[27,28] Our study reveals that the interaction mode between BtHKU5-CoV-2-441 RBD and human ACE2 is considerably different from previously known ACE2-using CoVs. However, the BtHKU5-CoV-2-441 RBD binds wide overlapping regions on human ACE2 with SARS-CoV-2 and NL63, underscoring this hot spot frequently opted by various CoVs. Recent preprints have reported that HKU5-CoV-1 engages ACE2 from the virus host *P.abr* bat as a receptor, with a binding mode similar to the mode used by HKU5-CoV-2.[30,31] However, structure comparison analysis reveals that numerous polar interactions cannot be achieved with human ACE2 by HKU5-CoV-1 RBD due to the presence of distinct residues. For instance, residue D329 in P. abr ACE2 forms a salt bridge with residue K544 in HKU5-CoV-1, an interaction that is not possible with the residue N330 of human ACE2. Additionally, residue K520 of HKU5-CoV-1 forms polar interactions with the residue N386 of *P.abr* ACE2 side chain, but in human ACE2, the corresponding residue is alanine. This observation is in concordance with the findings from the team led by David Veesler.[31] In our study, mutagenesis analysis based on the BtHKU5-CoV-2-441 RBD-hACE2 complex structure suggests that a better adaptation of BtHKU5-CoV-2-441 RBD to human ACE2. Efficient engagement with human ACE2 and the broader host spectrum in terms of ACE2 ortholog tropism imply a higher spillover risk for BtHKU5-CoV-2 compared with lineage 1 HKU5-CoVs.[31] However, the human ACE2-binding affinity of BtHKU5-CoV-2-441 is significantly lower than SARS-CoV-2.[34] S protein of BtHKU5-CoV-2-441 is not efficiently cleaved as MERS-CoV during biogenesis, and exogenous trypsin treatment enhances this cleavage and cell entry efficiency (Figure S6N). Due to these suboptimal factors for human adaptation, the risk of BtHKU5-CoV-2 emergence in human populations should not be exaggerated.

CoVs exhibit high genetic diversity in wildlife and rapidly evolve and adapt to the new hosts during interspecies transmission or when circulating within high-density populations. Developing countermeasures, including diagnosis tools, antiviral drugs, and pan-CoV vaccines, targeting multiple viral species, genus, or even family, will be helpful for preventing the pandemic of the next "disease X" caused by CoVs. In this study, we identified that the monoclonal antibodies 76E1 and S2P6, which targets the SARS-CoV-2 S2 protein, and one pan-CoV fusion inhibitor EK1C4 and three small molecules nirmatrelvir, remdesivir, and GC376 showed antiviral potency against HKU5-CoV-2, highlighting their potential as therapeutic candidates against those merbecoviruses.

Limitations of the study

While we demonstrated that BtHKU5-CoV-2 utilized human ACE2 as cell receptor and host proteases played a role in cell entry, this study had several limitations. First, although we demonstrated human ACE2 utilization of BtHKU5-CoV-2 using stains BtHKU5-CoV-2-441 and BtHKU5-CoV-2-023, further investigation is necessary to examine whether other BtHKU5-CoV-2 strains with genetic diversity in their S protein sequences have better ACE2 adaptation. Second, while we demonstrated that the cleavage sites in S1/S2 and S2′ of BtHKU5-CoV-2 S protein are important for S protein priming and membrane fusion, the detailed mechanism of host-protease-mediated S proteolytic activation has not been clearly elucidated. Finally, the potential and consequences of BtHKU5-CoV-2 infection has not been evaluated *in vivo*. Given their potential broad host range and relatively high human infection risks, the pathogenicity of BtHKU5-CoV-2 should be evaluated in animal models, such as hamsters and human ACE2 transgenic mice in future studies.

RESOURCE AVAILABILITY

Lead contact

Further information and requests for resources and reagents should be directed to and will be fulfilled by the lead contact, Zheng-Li Shi (shi_zhengli@gzlab.ac.cn).

Materials availability

The materials used and generated in this study are available from the lead contact upon reasonable request with a completed material transfer agreement.

Data and code availability

- The NGS raw data and the full-length genome sequences of BtHKU5-CoV-2-153, BtHKU5-CoV-2-155, BtHKU5-CoV-2-023, BtHKU5-CoV-2-028, BtHKU5-CoV-2-381, and BtHKU5-CoV-2-441 have been submitted to NGDC (National Genomics Data Center) database. The NGS raw data have been submitted to GSA (Genome Sequence Archive) with original code: CRA018893. The full-length genome sequences have been submitted to GenBase with accession numbers: C_AA085189.1, C_AA085190.1, C_AA085191.1, C_AA085192.1, C_AA085193.1, and C_AA085194.1.
- The cryo-EM map has been deposited at the Electron Microscopy Data Bank (EMDB) under the following accession numbers: EMD-61517 (BtHKU5-CoV-2-441 RBD–hACE2 complex). Atomic model corresponding to EMD-61517 has been deposited at the Protein Data Bank (PDB) and are available under the accession number of 9JJ6.
- Any additional information required to analyze the data reported in this paper is available from the lead contact upon request.

ACKNOWLEDGMENTS

We thank Youchun Wang (National Institutes for Food and Drug Control) for his kind offer of cell-cell fusion assay system. We thank Qiang Ding (Tsinghua University) for his kind offer of some mammalian ACE2 plasmids. We thank Lu Lu and Shuai Xia (Fudan University) for his kind offer of EK1C4. We thank Rui Gong (Wuhan Institute of Virology) for his kind offer of m336 antibody. We thank Lu Peng (Wuhan Institute of Virology) and Yanni Shu (Wuhan Institute of Virology) for their kind offer of monoclonal antibody anti-S tag. Images used in schematic model and graphical abstract are adapted from BioRender. This study was supported by funding from the National Key R&D Program of China (2023YFC2605500 to Z.-L.S. and H.Y.; 2022YFC2305101 to B.H.), Guangzhou Laboratory (SRPG22-001 to Z.-L.S. and P.Z.; GZNL2023A01001 to Z.-L.S.; SRPG22-003 to W.P.), the National Natural Science Foundation of China (2361133556 to Z.-L.S.; 32300137 to J.C.; 32100142 to W.Z.; 82300014 to Y.L.; 82322041 and 32270164 to H.Y.; 32370464 to L.Z.; 323B2006 to C.-B.M.), the Natural Science Foundation of Hubei Province (2024AFB843 to J.C.; 2023AFA015 to H.Y.), and TaiKang Center for Life and Medical Sciences (to H.Y.).

Please cite this article in press as: Chen et al., Bat-infecting merbecovirus HKU5-CoV lineage 2 can use human ACE2 as a cell entry receptor, Cell (2025), https://doi.org/10.1016/j.cell.2025.01.042

AUTHOR CONTRIBUTIONS

Z.-L.S., W.P., P.Z., H.Y., and J.C. conceived the project and prepared the manuscript. J.C., Y.L., C.L., and C.-B.M. performed the pseudovirus experiments. Y.L. performed viral isolation and authentic virus experiments. W.Z. and H.C. carried out the cryo-EM sample preparation, data collection, and processing of the protein complex and built and refined the BtHKU5-CoV-2-441 RBD-hACE2 complex structure. L.Z. and X.H. conducted the sample collection. T.D., C.W., J.S., B.L., and Y.Z. performed genome sequencing, annotations, and sequence analysis. W.Z. and H.C. performed protein purification and SPR assay. J.J. and Z.G. established human ACE2 knockout cell lines and host protease knockdown cell lines. C.-B.M., C.L., K.P., and H.L. generate clones. C.L., A.L., and W.Z. provided help for experiments.

DECLARATION OF INTERESTS

The authors declare no competing interests.

STAR★METHODS

Detailed methods are provided in the online version of this paper and include the following:

- KEY RESOURCES TABLE
- EXPERIMENTAL MODEL AND STUDY PARTICIPANT DETAILS
  - Cell lines
  - Human organoids
  - Bat samples
  - Biosafety statement
- METHOD DETAILS
  - Coronavirus identification and sequencing
  - Phylogenetic analysis
  - Pseudovirus production and transduction
  - Cell-cell fusion assay
  - RBD-hFc live-cell binding assay
  - Establishment of the *hACE2*-knockout cell line
  - Western blot
  - Protein expression and purification
  - SPR
  - Cryo-EM sample preparation and data collection
  - Imaging processing
  - Model building and refinement
  - Virus isolation
  - Immunofluorescence staining
  - Infection in human organoids
  - RNA extraction and qRT-PCR
  - ACE2 blocking assay
  - Protease inhibition
  - Neutralization assays
- QUANTIFICATION AND STATISTICAL ANALYSIS

SUPPLEMENTAL INFORMATION

Supplemental information can be found online at https://doi.org/10.1016/j.cell.2025.01.042.

Received: September 17, 2024
Revised: December 16, 2024
Accepted: January 29, 2025
Published: February 18, 2025

REFERENCES

1. Guan, Y., Zheng, B.J., He, Y.Q., Liu, X.L., Zhuang, Z.X., Cheung, C.L., Luo, S.W., Li, P.H., Zhang, L.J., Guan, Y.J., et al. (2003). Isolation and characterization of viruses related to the SARS coronavirus from animals in southern China. Science *302*, 276–278. https://doi.org/10.1126/science.1087139.
2. Azhar, E.I., El-Kafrawy, S.A., Farraj, S.A., Hassan, A.M., Al-Saeed, M.S., Hashem, A.M., and Madani, T.A. (2014). Evidence for camel-to-human transmission of MERS coronavirus. N. Engl. J. Med. *370*, 2499–2505. https://doi.org/10.1056/NEJMoa1401505.
3. Temmam, S., Vongphayloth, K., Baquero, E., Munier, S., Bonomi, M., Regnault, B., Douangboubpha, B., Karami, Y., Chrétien, D., Sanamxay, D., et al. (2022). Bat coronaviruses related to SARS-CoV-2 and infectious for human cells. Nature *604*, 330–336. https://doi.org/10.1038/s41586-022-04532-4.
4. Li, W., Shi, Z., Yu, M., Ren, W., Smith, C., Epstein, J.H., Wang, H., Crameri, G., Hu, Z., Zhang, H., et al. (2005). Bats are natural reservoirs of SARS-like coronaviruses. Science *310*, 676–679. https://doi.org/10.1126/science.1118391.
5. Hu, B., Zeng, L.P., Yang, X.L., Ge, X.Y., Zhang, W., Li, B., Xie, J.Z., Shen, X.R., Zhang, Y.Z., Wang, N., et al. (2017). Discovery of a rich gene pool of bat SARS-related coronaviruses provides new insights into the origin of SARS coronavirus. PLoS Pathog. *13*, e1006698. https://doi.org/10.1371/journal.ppat.1006698.
6. Ithete, N.L., Stoffberg, S., Corman, V.M., Cottontail, V.M., Richards, L.R., Schoeman, M.C., Drosten, C., Drexler, J.F., and Preiser, W. (2013). Close relative of human Middle East respiratory syndrome coronavirus in bat, South Africa. Emerg Infect Dis *19*, 1697–1699. https://doi.org/10.3201/eid1910.130946.
7. Luo, C.M., Wang, N., Yang, X.L., Liu, H.Z., Zhang, W., Li, B., Hu, B., Peng, C., Geng, Q.B., Zhu, G.J., et al. (2018). Discovery of Novel Bat Coronaviruses in South China That Use the Same Receptor as Middle East Respiratory Syndrome Coronavirus. J. Virol. *92*. e00116–18. https://doi.org/10.1128/JVI.00116-18.
8. Zhou, P., Yang, X.L., Wang, X.G., Hu, B., Zhang, L., Zhang, W., Si, H.R., Zhu, Y., Li, B., Huang, C.L., et al. (2020). A pneumonia outbreak associated with a new coronavirus of probable bat origin. Nature *579*, 270–273. https://doi.org/10.1038/s41586-020-2012-7.
9. Lau, S.K.P., Fan, R.Y.Y., Zhu, L., Li, K.S.M., Wong, A.C.P., Luk, H.K.H., Wong, E.Y.M., Lam, C.S.F., Lo, G.C.S., Fung, J., et al. (2021). Isolation of MERS-related coronavirus from lesser bamboo bats that uses DPP4 and infects human-DPP4-transgenic mice. Nat. Commun. *12*, 216. https://doi.org/10.1038/s41467-020-20458-9.
10. Tse, L.V., Hou, Y.J., McFadden, E., Lee, R.E., Scobey, T.D., Leist, S.R., Martinez, D.R., Meganck, R.M., Schäfer, A., Yount, B.L., et al. (2023). A MERS-CoV antibody neutralizes a pre-emerging group 2c bat coronavirus. Sci. Transl. Med. *15*, eadg5567. https://doi.org/10.1126/scitranslmed.adg5567.
11. Lau, S.K.P., Zhang, L., Luk, H.K.H., Xiong, L., Peng, X., Li, K.S.M., He, X., Zhao, P.S.H., Fan, R.Y.Y., Wong, A.C.P., et al. (2018). Receptor Usage of a Novel Bat Lineage C Betacoronavirus Reveals Evolution of Middle East Respiratory Syndrome-Related Coronavirus Spike Proteins for Human Dipeptidyl Peptidase 4 Binding. J. Infect. Dis. *218*, 197–207. https://doi.org/10.1093/infdis/jiy018.
12. Chen, J., Yang, X., Si, H., Gong, Q., Que, T., Li, J., Li, Y., Wu, C., Zhang, W., Chen, Y., et al. (2023). A bat MERS-like coronavirus circulates in pangolins and utilizes human DPP4 and host proteases for cell entry. Cell *186*, 850–863.e16. https://doi.org/10.1016/j.cell.2023.01.019.
13. Shi, W., Shi, M., Que, T.C., Cui, X.M., Ye, R.Z., Xia, L.Y., Hou, X., Zheng, J.J., Jia, N., Xie, X., et al. (2022). Trafficked Malayan pangolins contain viral pathogens of humans. Nat. Microbiol. *7*, 1259–1269. https://doi.org/10.1038/s41564-022-01181-1.
14. Cui, X., Fan, K., Liang, X., Gong, W., Chen, W., He, B., Chen, X., Wang, H., Wang, X., Zhang, P., et al. (2023). Virus diversity, wildlife-domestic animal circulation and potential zoonotic viruses of small mammals, pangolins and zoo animals. Nat. Commun. *14*, 2488. https://doi.org/10.1038/s41467-023-38202-4.
15. Zhao, J., Wan, W., Yu, K., Lemey, P., Pettersson, J.H.O., Bi, Y., Lu, M., Li, X., Chen, Z., Zheng, M., et al. (2024). Farmed fur animals harbour viruses

Please cite this article in press as: Chen et al., Bat-infecting merbecovirus HKU5-CoV lineage 2 can use human ACE2 as a cell entry receptor, Cell (2025), https://doi.org/10.1016/j.cell.2025.01.042

with zoonotic spillover potential. Nature *634*, 228–233. https://doi.org/10.1038/s41586-024-07901-3.

16. Li, F. (2016). Structure, Function, and Evolution of Coronavirus Spike Proteins. Annu. Rev. Virol. *3*, 237–261. https://doi.org/10.1146/annurev-virology-110615-042301.
17. Li, F. (2015). Receptor recognition mechanisms of coronaviruses: a decade of structural studies. J. Virol. *89*, 1954–1964. https://doi.org/10.1128/JVI.02615-14.
18. Raj, V.S., Mou, H., Smits, S.L., Dekkers, D.H.W., Müller, M.A., Dijkman, R., Muth, D., Demmers, J.A.A., Zaki, A., Fouchier, R.A.M., et al. (2013). Dipeptidyl peptidase 4 is a functional receptor for the emerging human coronavirus-EMC. Nature *495*, 251–254. https://doi.org/10.1038/nature12005.
19. Li, W., Moore, M.J., Vasilieva, N., Sui, J., Wong, S.K., Berne, M.A., Somasundaran, M., Sullivan, J.L., Luzuriaga, K., Greenough, T.C., et al. (2003). Angiotensin-converting enzyme 2 is a functional receptor for the SARS coronavirus. Nature *426*, 450–454. https://doi.org/10.1038/nature02145.
20. Yeager, C.L., Ashmun, R.A., Williams, R.K., Cardellichio, C.B., Shapiro, L.H., Look, A.T., and Holmes, K.V. (1992). Human aminopeptidase N is a receptor for human coronavirus 229E. Nature *357*, 420–422. https://doi.org/10.1038/357420a0.
21. Williams, R.K., Jiang, G.S., and Holmes, K.V. (1991). Receptor for mouse hepatitis virus is a member of the carcinoembryonic antigen family of glycoproteins. Proc. Natl. Acad. Sci. USA *88*, 5533–5536. https://doi.org/10.1073/pnas.88.13.5533.
22. Saunders, N., Fernandez, I., Planchais, C., Michel, V., Rajah, M.M., Baquero Salazar, E., Postal, J., Porrot, F., Guivel-Benhassine, F., Blanc, C., et al. (2023). TMPRSS2 is a functional receptor for human coronavirus HKU1. Nature *624*, 207–214. https://doi.org/10.1038/s41586-023-06761-7.
23. Hofmann, H., Pyrc, K., van der Hoek, L., Geier, M., Berkhout, B., and Pöhlmann, S. (2005). Human coronavirus NL63 employs the severe acute respiratory syndrome coronavirus receptor for cellular entry. Proc. Natl. Acad. Sci. USA *102*, 7988–7993. https://doi.org/10.1073/pnas.0409465102.
24. Guo, H., Li, A., Dong, T.Y., Si, H.R., Hu, B., Li, B., Zhu, Y., Shi, Z.L., and Letko, M. (2023). Isolation of ACE2-dependent and -independent sarbecoviruses from Chinese horseshoe bats. J. Virol. *97*, e0039523. https://doi.org/10.1128/jvi.00395-23.
25. Xiong, Q., Ma, C., Liu, C., Tong, F., Huang, M., and Yan, H. (2024). ACE2-using merbecoviruses: Further evidence of convergent evolution of ACE2 recognition by NeoCoV and other MERS-CoV related viruses. Cell Insight *3*, 100145. https://doi.org/10.1016/j.cellin.2023.100145.
26. Wang, Q., Qi, J., Yuan, Y., Xuan, Y., Han, P., Wan, Y., Ji, W., Li, Y., Wu, Y., Wang, J., et al. (2014). Bat origins of MERS-CoV supported by bat coronavirus HKU4 usage of human receptor CD26. Cell Host Microbe *16*, 328–337. https://doi.org/10.1016/j.chom.2014.08.009.
27. Xiong, Q., Cao, L., Ma, C., Tortorici, M.A., Liu, C., Si, J., Liu, P., Gu, M., Walls, A.C., Wang, C., et al. (2022). Close relatives of MERS-CoV in bats use ACE2 as their functional receptors. Nature *612*, 748–757. https://doi.org/10.1038/s41586-022-05513-3.
28. Ma, C.B., Liu, C., Park, Y.J., Tang, J.J., Chen, J., Xiong, Q., Lee, J., Stewart, C., Asarnow, D., Brown, J., et al. (2024). Multiple independent acquisitions of ACE2 usage in MERS-related coronaviruses. Preprint at biorxiv. https://doi.org/10.1101/2023.10.02.560486.
29. Ma, C., Liu, C., Xiong, Q., Gu, M., Shi, L., Wang, C., Si, J., Tong, F., Liu, P., Huang, M., et al. (2023). Broad host tropism of ACE2-using MERS-related coronaviruses and determinants restricting viral recognition. Cell Discov. *9*, 57. https://doi.org/10.1038/s41421-023-00566-8.
30. Catanzaro, N.J., Wu, Z.Y., Fan, C.C., Schäfer, A., Yount, B.L., Bjorkman, P.J., Baric, R.S., and Letko, M. (2024). ACE2 from Pipistrellus abramus bats is a receptor for HKU5 coronaviruses. Preprint at bioRxiv. https://doi.org/10.1101/2024.03.13.584892.
31. Park, Y.J., Liu, C., Lee, J.M., Brown, J.T., Ma, C.B., Liu, P., Xiong, Q., Stewart, C., Addetia, A., Craig, C.J., et al. (2024). Molecular basis of convergent evolution of ACE2 receptor utilization among HKU5 coronaviruses. Preprint at bioRxiv. https://doi.org/10.1101/2024.08.28.608351.
32. Latinne, A., Hu, B., Olival, K.J., Zhu, G., Zhang, L., Li, H., Chmura, A.A., Field, H.E., Zambrana-Torrelio, C., Epstein, J.H., et al. (2020). Origin and cross-species transmission of bat coronaviruses in China. Nat. Commun. *11*, 4235. https://doi.org/10.1038/s41467-020-17687-3.
33. International Committee on Taxonomy of Viruses Executive Committee (2020). The new scope of virus taxonomy: partitioning the virosphere into 15 hierarchical ranks. Nat. Microbiol. *5*, 668–674. https://doi.org/10.1038/s41564-020-0709-x.
34. Li, L., Liao, H., Meng, Y., Li, W., Han, P., Liu, K., Wang, Q., Li, D., Zhang, Y., Wang, L., et al. (2022). Structural basis of human ACE2 higher binding affinity to currently circulating Omicron SARS-CoV-2 sub-variants BA.2 and BA.1.1. Cell *185*, 2952–2960.e10. https://doi.org/10.1016/j.cell.2022.06.023.
35. Li, F., Li, W., Farzan, M., and Harrison, S.C. (2005). Structure of SARS coronavirus spike receptor-binding domain complexed with receptor. Science *309*, 1864–1868. https://doi.org/10.1126/science.1116480.
36. Wu, K., Li, W., Peng, G., and Li, F. (2009). Crystal structure of NL63 respiratory coronavirus receptor-binding domain complexed with its human receptor. Proc. Natl. Acad. Sci. USA *106*, 19970–19974. https://doi.org/10.1073/pnas.0908837106.
37. Du, Y., Shi, R., Zhang, Y., Duan, X., Li, L., Zhang, J., Wang, F., Zhang, R., Shen, H., Wang, Y., et al. (2021). A broadly neutralizing humanized ACE2-targeting antibody against SARS-CoV-2 variants. Nat. Commun. *12*, 5000. https://doi.org/10.1038/s41467-021-25331-x.
38. Shirato, K., Kawase, M., and Matsuyama, S. (2013). Middle East respiratory syndrome coronavirus infection mediated by the transmembrane serine protease TMPRSS2. J. Virol. *87*, 12552–12561. https://doi.org/10.1128/JVI.01890-13.
39. Drosten, C., Günther, S., Preiser, W., van der Werf, S., Brodt, H.R., Becker, S., Rabenau, H., Panning, M., Kolesnikova, L., Fouchier, R.A.M., et al. (2003). Identification of a novel coronavirus in patients with severe acute respiratory syndrome. N. Engl. J. Med. *348*, 1967–1976. https://doi.org/10.1056/NEJMoa030747.
40. Fouchier, R.A.M., Hartwig, N.G., Bestebroer, T.M., Niemeyer, B., de Jong, J.C., Simon, J.H., and Osterhaus, A.D.M.E. (2004). A previously undescribed coronavirus associated with respiratory disease in humans. Proc. Natl. Acad. Sci. USA *101*, 6212–6216. https://doi.org/10.1073/pnas.0400762101.
41. Ying, T., Du, L., Ju, T.W., Prabakaran, P., Lau, C.C.Y., Lu, L., Liu, Q., Wang, L., Feng, Y., Wang, Y., et al. (2014). Exceptionally potent neutralization of Middle East respiratory syndrome coronavirus by human monoclonal antibodies. J. Virol. *88*, 7796–7805. https://doi.org/10.1128/JVI.00912-14.
42. Hansen, J., Baum, A., Pascal, K.E., Russo, V., Giordano, S., Wloga, E., Fulton, B.O., Yan, Y., Koon, K., Patel, K., et al. (2020). Studies in humanized mice and convalescent humans yield a SARS-CoV-2 antibody cocktail. Science *369*, 1010–1014. https://doi.org/10.1126/science.abd0827.
43. Sun, X., Yi, C., Zhu, Y., Ding, L., Xia, S., Chen, X., Liu, M., Gu, C., Lu, X., Fu, Y., et al. (2022). Neutralization mechanism of a human antibody with pan-coronavirus reactivity including SARS-CoV-2. Nat. Microbiol. *7*, 1063–1074. https://doi.org/10.1038/s41564-022-01155-3.
44. Pinto, D., Sauer, M.M., Czudnochowski, N., Low, J.S., Tortorici, M.A., Housley, M.P., Noack, J., Walls, A.C., Bowen, J.E., Guarino, B., et al. (2021). Broad betacoronavirus neutralization by a stem helix-specific human antibody. Science *373*, 1109–1116. https://doi.org/10.1126/science.abj3321.
45. Xia, S., Liu, M., Wang, C., Xu, W., Lan, Q., Feng, S., Qi, F., Bao, L., Du, L., Liu, S., et al. (2020). Inhibition of SARS-CoV-2 (previously 2019-nCoV) infection by a highly potent pan-coronavirus fusion inhibitor targeting its spike protein that harbors a high capacity to mediate membrane fusion. Cell Res. *30*, 343–355. https://doi.org/10.1038/s41422-020-0305-x.

Please cite this article in press as: Chen et al., Bat-infecting merbecovirus HKU5-CoV lineage 2 can use human ACE2 as a cell entry receptor, Cell (2025), https://doi.org/10.1016/j.cell.2025.01.042

46. Owen, D.R., Allerton, C.M.N., Anderson, A.S., Aschenbrenner, L., Avery, M., Berritt, S., Boras, B., Cardin, R.D., Carlo, A., Coffman, K.J., et al. (2021). An oral SARS-CoV-2 M(pro) inhibitor clinical candidate for the treatment of COVID-19. Science *374*, 1586–1593. https://doi.org/10.1126/science.abl4784.

47. Sheahan, T.P., Sims, A.C., Graham, R.L., Menachery, V.D., Gralinski, L.E., Case, J.B., Leist, S.R., Pyrc, K., Feng, J.Y., Trantcheva, I., et al. (2017). Broad-spectrum antiviral GS-5734 inhibits both epidemic and zoonotic coronaviruses. Sci. Transl. Med. *9*, eaal3653. https://doi.org/10.1126/scitranslmed.aal3653.

48. Rathnayake, A.D., Zheng, J., Kim, Y., Perera, K.D., Mackin, S., Meyerholz, D.K., Kashipathy, M.M., Battaile, K.P., Lovell, S., Perlman, S., et al. (2020). 3C-like protease inhibitors block coronavirus replication in vitro and improve survival in MERS-CoV-infected mice. Sci. Transl. Med. *12*, eabc5332. https://doi.org/10.1126/scitranslmed.abc5332.

49. Woo, P.C.Y., Lau, S.K.P., Li, K.S.M., Poon, R.W.S., Wong, B.H.L., Tsoi, H.W., Yip, B.C.K., Huang, Y., Chan, K.H., and Yuen, K.Y. (2006). Molecular diversity of coronaviruses in bats. Virology *351*, 180–187. https://doi.org/10.1016/j.virol.2006.02.041.

50. Wu, Z., Yang, L., Ren, X., He, G., Zhang, J., Yang, J., Qian, Z., Dong, J., Sun, L., Zhu, Y., et al. (2016). Deciphering the bat virome catalog to better understand the ecological diversity of bat viruses and the bat origin of emerging infectious diseases. ISME J. *10*, 609–620. https://doi.org/10.1038/ismej.2015.138.

51. Lee, S., Jo, S.D., Son, K., An, I., Jeong, J., Wang, S.J., Kim, Y., Jheong, W., and Oem, J.K. (2018). Genetic Characteristics of Coronaviruses from Korean Bats in 2016. Microb. Ecol. *75*, 174–182. https://doi.org/10.1007/s00248-017-1033-8.

52. Han, Y., Xu, P., Wang, Y., Zhao, W., Zhang, J., Zhang, S., Wang, J., Jin, Q., and Wu, Z. (2023). Panoramic analysis of coronaviruses carried by representative bat species in Southern China to better understand the coronavirus sphere. Nat. Commun. *14*, 5537. https://doi.org/10.1038/s41467-023-41264-z.

53. Ge, X.Y., Li, J.L., Yang, X.L., Chmura, A.A., Zhu, G., Epstein, J.H., Mazet, J.K., Hu, B., Zhang, W., Peng, C., et al. (2013). Isolation and characterization of a bat SARS-like coronavirus that uses the ACE2 receptor. Nature *503*, 535–538. https://doi.org/10.1038/nature12711.

54. Guo, H., Hu, B., Si, H.R., Zhu, Y., Zhang, W., Li, B., Li, A., Geng, R., Lin, H.F., Yang, X.L., et al. (2021). Identification of a novel lineage bat SARS-related coronaviruses that use bat ACE2 receptor. Emerg. Microbes Infect. *10*, 1507–1514. https://doi.org/10.1080/22221751.2021.1956373.

55. Wrobel, A.G., Benton, D.J., Xu, P., Calder, L.J., Borg, A., Roustan, C., Martin, S.R., Rosenthal, P.B., Skehel, J.J., and Gamblin, S.J. (2021). Structure and binding properties of Pangolin-CoV spike glycoprotein inform the evolution of SARS-CoV-2. Nat. Commun. *12*, 837. https://doi.org/10.1038/s41467-021-21006-9.

56. Gong, Q., Jiang, R., Ji, L., Lin, H., Liu, M., Tang, X., Yang, Y., Han, W., Chen, J., Guo, Z., et al. (2024). Establishment of a human organoid-based evaluation system for assessing interspecies infection risk of animal-borne coronaviruses. Emerg. Microbes Infect. *13*, 2327368. https://doi.org/10.1080/22221751.2024.2327368.

57. Zhou, P., Fan, H., Lan, T., Yang, X.L., Shi, W.F., Zhang, W., Zhu, Y., Zhang, Y.W., Xie, Q.M., Mani, S., et al. (2018). Fatal swine acute diarrhoea syndrome caused by an HKU2-related coronavirus of bat origin. Nature *556*, 255–258. https://doi.org/10.1038/s41586-018-0010-9.

58. Liu, Y., Hu, G., Wang, Y., Ren, W., Zhao, X., Ji, F., Zhu, Y., Feng, F., Gong, M., Ju, X., et al. (2021). Functional and genetic analysis of viral receptor ACE2 orthologs reveals a broad potential host range of SARS-CoV-2. Proc. Natl. Acad. Sci. USA *118*, e2025373118. https://doi.org/10.1073/pnas.2025373118.

59. Nguyen, L.T., Schmidt, H.A., von Haeseler, A., and Minh, B.Q. (2015). IQ-TREE: a fast and effective stochastic algorithm for estimating maximum-likelihood phylogenies. Mol. Biol. Evol. *32*, 268–274. https://doi.org/10.1093/molbev/msu300.

60. Katoh, K., Misawa, K., Kuma, K., and Miyata, T. (2002). MAFFT: a novel method for rapid multiple sequence alignment based on fast Fourier transform. Nucleic Acids Res. *30*, 3059–3066. https://doi.org/10.1093/nar/gkf436.

61. Punjani, A., Rubinstein, J.L., Fleet, D.J., and Brubaker, M.A. (2017). cryoSPARC: algorithms for rapid unsupervised cryo-EM structure determination. Nat. Methods *14*, 290–296. https://doi.org/10.1038/nmeth.4169.

62. Emsley, P., Lohkamp, B., Scott, W.G., and Cowtan, K. (2010). Features and development of coot. Acta Crystallogr. D Biol. Crystallogr. *66*, 486–501. https://doi.org/10.1107/S0907444910007493.

63. Afonine, P.V., Grosse-Kunstleve, R.W., Echols, N., Headd, J.J., Moriarty, N.W., Mustyakimov, M., Terwilliger, T.C., Urzhumtsev, A., Zwart, P.H., and Adams, P.D. (2012). Towards automated crystallographic structure refinement with phenix.refine. Acta Crystallogr. D Biol. Crystallogr. *68*, 352–367. https://doi.org/10.1107/S0907444912001308.

64. Davis, I.W., Leaver-Fay, A., Chen, V.B., Block, J.N., Kapral, G.J., Wang, X., Murray, L.W., Arendall, W.B., 3rd, Snoeyink, J., Richardson, J.S., and Richardson, D.C. (2007). MolProbity: all-atom contacts and structure validation for proteins and nucleic acids. Nucleic Acids Res. *35*, W375–W383. https://doi.org/10.1093/nar/gkm216.

65. Pettersen, E.F., Goddard, T.D., Huang, C.C., Couch, G.S., Greenblatt, D.M., Meng, E.C., and Ferrin, T.E. (2004). UCSF Chimera–a visualization system for exploratory research and analysis. J. Comput. Chem. *25*, 1605–1612. https://doi.org/10.1002/jcc.20084.

66. Pettersen, E.F., Goddard, T.D., Huang, C.C., Meng, E.C., Couch, G.S., Croll, T.I., Morris, J.H., and Ferrin, T.E. (2021). UCSF ChimeraX: Structure visualization for researchers, educators, and developers. Protein Sci. *30*, 70–82. https://doi.org/10.1002/pro.3943.

67. Zhang, L., Li, Q., Wu, J., Yu, Y., Zhang, Y., Nie, J., Liang, Z., Cui, Z., Liu, S., Wang, H., et al. (2022). Analysis of SARS-CoV-2 variants B.1.617: host tropism, proteolytic activation, cell-cell fusion, and neutralization sensitivity. Emerg. Microbes Infect. *11*, 1024–1036. https://doi.org/10.1080/22221751.2022.2054369.

Please cite this article in press as: Chen et al., Bat-infecting merbecovirus HKU5-CoV lineage 2 can use human ACE2 as a cell entry receptor, Cell (2025), https://doi.org/10.1016/j.cell.2025.01.042

CellPress

STAR★METHODS

KEY RESOURCES TABLE

REAGENT or RESOURCE	SOURCE	IDENTIFIER
Antibodies		
Goat Anti-Rabbit IgG H&L (Cy3) preadsorbed	Abcam	Cat#: ab6939; RRID: AB_955021
Goat Anti-Mouse IgG H&L (Alexa Fluor 488) preadsorbed	Abcam	Cat#: ab150117; RRID: AB_2688012
Alexa Fluor 594 conjugated goat anti-mouse IgG	Abcam	Cat#: ab150120: RRID: AB_2631447
DYKDDDDK-Tag(3B9) mAb (Same as Sigma's Anti-FLAG M2)	Abmart	Cat#: M20008L
Anti-VSV-G [8G5F11] Antibody	Kerafast	Cat#: EB0010; RRID: AB_2811223
Anti-VSV-M [23H12] Antibody	Kerafast	Cat#: EB0011; RRID: AB_2734773
GAPDH Monoclonal antibody	Proteintech	Cat#: 60004-1-Ig; RRID: AB_2107436
HRP-conjugated Affinipure Goat Anti-Mouse IgG(H+L)	Proteintech	Cat#: SA00001-1; RRID: AB_2722565
Human/Mouse/Rat/Hamster ACE-2 Antibody	R&D systems	Cat#: AF933; RRID: AB_355722
Alexa Fluor 488-conjugated goat anti- human IgG	Thermo Fisher Scientific	Cat#: A11013; RRID: AB_141360
Mouse anti-FLAG antibody M2	Sigma-Aldrich	Cat#: F1804; RRID: AB_262044
Alexa Fluor 594-conjugated goat anti- mouse IgG	Thermo Fisher Scientific	Cat#: A32742; RRID: AB_2762825
Rabbit anti-BtHKU5-CoV-2-441 N protein polyclonal antibody	This paper	N/A
Mouse anti-S tag monoclonal antibody	Zhou et al.[8]	N/A
m336	Ying et al.[41]	N/A
76E1	Sun et al.[43]	N/A
S2P6	Pinto et al.[44]	N/A
REGN10933	Hansen et al.[42]	N/A
REGN10987	Hansen et al.[42]	N/A
h11B11	Du et al.[37]	N/A
Bacterial and virus strains		
BtHKU5-CoV-2-023	Isolated from bat anal swab sample	N/A
VSV* △G-FLuc	Guo et al.[54]	N/A
Biological samples		
Bat anal swab sample	This paper	N/A
Chemicals, peptides, and recombinant proteins		
Lipofectamine 3000	Thermo Fisher Scientific	Cat#: L3000015
DAPI	Beyotime	Cat#: C1002
4% paraformaldehyde	Boster	Cat#: AR1068
Furin inhibitor, decanoyl-RVKR-CMK	Tocris	Cat#: 3501
Camostat	MedChemExpress	Cat#: HY-13512
Aloxistatin (E64d)	Selleck	Cat#: S7393
Hydroxychloroquine sulfate	Tocris	Cat#: 5648
Bafilomycin A1	Sangon Biotech	Cat#: A601116
BtHKU5-CoV-2-441 RBD	This paper	N/A
Human ACE2	This paper	N/A
SARS-CoV-2 RBD	This paper	N/A
SARS-CoV RBD	This paper	N/A
MERS-CoV RBD	This paper	N/A
VeZol Reagent	Vazyme	Cat#: R411-02
Matrigel	CORNING	Cat#: 356231
TPCK-treated trypsin	Sigma-Aldrich	Cat#: T8802

(*Continued on next page*)

Please cite this article in press as: Chen et al., Bat-infecting merbecovirus HKU5-CoV lineage 2 can use human ACE2 as a cell entry receptor, Cell (2025), https://doi.org/10.1016/j.cell.2025.01.042

Continued

REAGENT or RESOURCE	SOURCE	IDENTIFIER
Hanks' Balanced Salt Solution	ServiceBio	Cat#: G4204
Poly-L-lysine hydrobromide	Sigma	Cat#: P1399
Nirmatrelvir	Selleck	Cat#: S9866
Remdersivir	Selleck	Cat#: S8932
GC376	Selleck	Cat#: S0475
EK1C4	Xia et al.[45]	N/A
Critical commercial assays		
Renilla Luciferase Assay System	Promega	Cat#: E2820
HiSxript II One step qRT-PCR SYBR Green Kit	Vazyme	Cat#: Q221-01
Bright-Lite Luciferase Assay System	Vazyme	Cat#: DD1204
VAMNE Virus DNA/RNA Extraction Kit	Vazyme	Cat#: RM501-01
SMARTER RACE 5'/3' Kit	Takara	Cat#: 634858
Deposited data		
Raw sequencing reads	This paper	NGDC-GSA: CRA018893
Viral genomes data	This paper	NGDC-GenBase: C_AA085189.1, C_AA085190.1, C_AA085191.1, C_AA085192.1, C_AA085193.1, C_AA085194.1
Atomic model of BtHKU5-CoV-2-441 RBD-hACE2 complex	This paper	PDB: 9JJ6
cryo-EM map of BtHKU5-CoV-2-441 RBD-hACE2 complex	This paper	EMDB: EMD-61517
Experimental models: Cell lines		
Caco-2	ATCC	ATCC Cat#: HTB-37; RRID: CVCL_0025
Huh-7	Laboratory of Xinwen Chen, Wuhan Institute of Virology	RRID: CVCL_0336
HEK293	Laboratory of Linfa Wang, Duke-NUS Medical School	ATCC Cat#: CRL-1573; RRID: CVCL_0045
HEK293-hACE2	Laboratory of Linfa Wang, Duke-NUS Medical School	N/A
Huh7.5.1	Laboratory of Jin Zhong, Shanghai Institute of Immunity and Infection	N/A
Huh-7 ACE2 KO	This paper	N/A
Caco-2 ACE2 KO	This paper	N/A
Caco-2-hACE2	This paper	N/A
HEK293T	ATCC	Cat#: CRL-11268
Caco-2-hACE2 TMPRSS2 KD	This paper	N/A
Caco-2-hACE2 Cathepsin L KD	This paper	N/A
Caco-2-hACE2 Furin KD	This paper	N/A
I1-Hybridoma cell lines	ATCC	Cat#: CRL-2700
Sf9 insect cells	GIBCO	N/A
Hi5 insect cells	GIBCO	N/A
HEK293F cells	GIBCO	N/A
Experimental models: Organisms/strains		
Human airway/nasal/colon organoids	Gong et al.[56] and Chen et al.[12]	N/A
Oligonucleotides		
F-BtHKU5-2-ORF1ab TCGTCAGTACCACCAGAAGA	This paper	N/A

(*Continued on next page*)

Please cite this article in press as: Chen et al., Bat-infecting merbecovirus HKU5-CoV lineage 2 can use human ACE2 as a cell entry receptor, Cell (2025), https://doi.org/10.1016/j.cell.2025.01.042

Continued

REAGENT or RESOURCE	SOURCE	IDENTIFIER
R-BtHKU5-2-ORF1ab CATAAAGTCCCACCCACCATAG	This paper	N/A
sgRNA target *hACE2* gene TGAGCAGGGAGGCATCCAAT	This paper	N/A
sgRNA target *hACE2* gene TGCTGCTCAGTCCACCATTG	This paper	N/A
Recombinant DNA		
Plasmid: pcDNA3.1-BtHKU5CoV-2-441-S-Stag	This paper	N/A
Plasmid: pCMV-3Tag-8-Human DPP4	Chen et al.[12]	N/A
Plasmid: pCAGGS-Human ACE2	Zhou et al.[57]	N/A
Plasmid: pCAGGS-Human APN	Zhou et al.[57]	N/A
Plasmid: pCAGGS-Human CEACAM1	This paper	N/A
Plasmid: pcDNA3.1-MERS-S-Stag	Chen et al.[12]	N/A
Plasmid: pcDNA3.1-HKU5-1-S-Stag	This paper	N/A
Plasmid: pcDNA3.1-BJ01-S-Stag	This paper	N/A
Plasmid: pcDNA3.1-SARS-CoV-2-S-Stag	This paper	N/A
Plasmid: pcDNA3.1-HKU4-CoV-S-Stag	Chen et al.[12]	N/A
Plasmid: pCMV-3Tag-8-Human furin	Chen et al.[12]	N/A
Plasmid: pcDNA3.1-HKU5-441-S-S1/S2mut-Stag	This paper	N/A
Plasmid: pcDNA3.1-HKU5-441-S- S2'mut-Stag	This paper	N/A
Plasmids: pLVX-EF1α-IRES-Puro-ACE2 othologs	Liu et al.[58] and Xiong et al.[27]	N/A
Plasmids: pCAGGS-ACE2 othologs	This paper	N/A
Plasmid: hACE2-pFastBac	This Paper	N/A
Plasmid: BtHKU5-CoV-2-441 RBD- pFastBac	This Paper	N/A
Plasmid: BtHKU5-CoV-2-441 RBD mutations-pcDNA3.1	This Paper	N/A
Software and algorithms		
figtree (v1.4.3)	Andrew Rambaut	http://tree.bio.ed.ac.uk/software/Figtree/
IQ-TREE (v2.3.5)	Barbetti et al.[59]	http://www.iqtree.org/about/
mafft (v7.525)	Katoh et al.[60]	https://mafft.cbrc.jp/alignment/software/
GraphPad Prism (version 10.2.0)	GraphPad Software	https://www.graphpad.com/
Cryosparc (Version 4.0.1)	Punjani et al.[61]	https://cryosparc.com/
Coot (v.0.9.6)	Emsley et al.[62]	https://www.ccp4.ac.uk/download/#os=windows
Phenix (v.1.20)	Afonine et al.[63]	https://phenix-online.org/
MolProbity	Davis et al.[64]	http://molprobity.biochem.duke.edu/
UCSF Chimera	Pettersen et al.[65]	https://www.cgl.ucsf.edu/chimera/
UCSF Chimera X	Pettersen et al.[66]	https://www.cgl.ucsf.edu/chimerax/
Other		
CM5	cytiva	BR100530

EXPERIMENTAL MODEL AND STUDY PARTICIPANT DETAILS

Cell lines

HEK293T cells were cultured in Dulbecco's modified Eagle medium (DMEM, Gibco) supplemented with 10% fetal bovine serum (FBS, Gibco). Huh-7.5.1 cells were kindly provided by Prof. Jin Zhong (Shanghai Institute of Immunity and Infection) and cultured in DMEM supplemented with 10% FBS. HEK293 cells and HEK293 cells that stably express human ACE2 (HEK293-hACE2) were kindly gifted from Prof. Lin-Fa Wang (Duke-NUS Medical School) and cultured in DMEM supplemented with 10% FBS. Caco-2 and Caco-2 cells stably express human ACE2 (Caco-2-hACE2) generated by lentivirus transduction and antibiotic selection were cultured in Eagle's Minimum Essential Medium (MEM, Gibco) supplemented with 10% FBS. Human ACE2 knock-out Huh-7 (Huh-7 ACE2 KO) cells and Caco-2 (Caco-2 ACE2 KO) cells were established using CRISPR-Cas9 system and cultured in DMEM

or MEM supplemented with 10% FBS, respectively. TMPRSS2, Cathepthin L and furin knock down Caco-2-hACE2 cells were established using CRISPR-Cas9 system and cultured in MEM supplemented with 10% FBS. All cell lines were cultured at a 37°C and 5% CO_2 incubator.

Human organoids

Human airway, nasal and colon organoids have been established in previous study.[56] For culturing theses human organoids, the cells were resuspended in cold Matrigel (Corning) and seeded in 24-well plates. After solidification of Matrigel, 500 μL organoid medium was added to each well and cells were cultured in a humidified 5% CO_2 incubator at 37°C. The medium was refreshed every three days and organoids were passaged every two weeks to sustain their growth and functionality.

Bat samples

A total of 954 *Pipistrellus* bat anal swab samples were collected from Guangdong, Fujian, Zhejiang, Anhui, Guangxi provinces in China as previously described.[4] The samples were transported and stored following standard procedures at the Wuhan Institute of Virology, Chinese Academy of Sciences.

Biosafety statement

Experiments related to virus isolation and cell assays of BtHKU5-CoV-2-023 were performed in a BSL-2 plus negative pressure following SOPs with necessary personal protection and approved by the Wuhan Institute of Virology (WIV) IBCs according to a biorisk assessment procedure (including the viral genome sequence and its phylogenetic relationship to known human viruses, human receptor utilization, cell tropism, prevalence in domestic animals and humans, and pathogenicity and transmission in animal models). All the facilities at WIV for this work adhere strictly to the safety requirements recommended by the China National Accreditation Service for Conformity Assessment. Biorisk assessment would be re-analyzed based on newly observed data of this virus to meet the necessary requirement of biocontainment levels.

METHOD DETAILS

Coronavirus identification and sequencing

Viral RNA was extracted from bat anal swab samples and used to detect CoV using pan-CoV detection primers targeting a 440-nt fragment of the *RdRp* gene, as previously described.[32] PCR products were gel purified and performed Sanger sequencing. The obtained sequences were confirmed through similarity analysis using the NCBI BLASTn search (http://www.ncbi.nlm.nih.gov/BLAST). NGS sequencing was performed by BGI. Sequence analysis was conducted as previously described.[8] RACE was performed using the SMARTER RACE 5' /3'Kit (Takara).

Phylogenetic analysis

To elucidate the evolutionary history and variation pattern of the new discovered *Pipistrellus* bat HKU5-CoV, phylogenetic trees were constructed using the whole genomes and the S protein amino acid sequences. Representative Alpha- and Betacoronaviruses were selected. Sequence alignments were performed by automatically selecting algorithm implemented in MAFFT (v7.525). Phylogenetic trees were inferred using the maximum likelihood (ML) method in iqtree (v2.3.5), employing the optimal fit substitution model, WAG+F+R5, for the S protein amino acid sequences and GTR+F+I+R5 for the genome sequences with 1000 bootstrap replicates. Phylogenetic trees were visualized using Figtree (v1.4.3).

Pseudovirus production and transduction

VSV pseudotyped viruses carrying foreign coronavirus S proteins were produced as previously discribed.[12] Firstly, pcDNA3.1 vectors containing respective S protein or empty vector were transfected into HEK293 cells by Lipofectamine 3000 transfection reagent (Invitrogen) according to the manufacturer's instruction. At 24 h post transfection (h.p.t.), the cells were transduced with VSV-△G-Fluc. After 2 h incubation, the inoculum was removed, and the cells were washed with DMEM and then added with DMEM containing VSV-G antibody (Kerafast, 1:1,000). Cells were further incubated for 48 h, the supernatant containing pseudotyped viruses was harvested, and cell debris was removed by centrifugation. Target cells were transduced with respective pseudotyped viruses with or without 0.5 μg/mL trypsin in the media without FBS. After 48 h post transduction, the luciferase substrate of Bright-Lite Luciferase Assay System (Vazyme) was added and the luciferase activity was measured using an Agilent BioTek Synergy H1 Multi-Mode Microplate Reader (BioTek).

Cell-cell fusion assay

Cell-cell fusion assay was conducted on HEK293 cells and HEK293-hACE2 cells as described previously.[67] Donor cells were HEK293 cells transfected with respective S protein expressing plasmid and the $GFP_{1-7}RL_N$ expressing plasmid. Acceptor HEK293-hACE2 cells were transfected with the $GFP_{8-11}RL_C$ expressing plasmid. At 24 h post transfection, donor cells and acceptor cells were detached, mixed at a ratio of 1:1 and plated into a 24-well plate with triplicate. Then 24 h later, fluorescent images were captured using a fluorescence microscope (Thermo Fisher Scientific). Meanwhile, cells were lysed and harvested to measure *Renilla*

Please cite this article in press as: Chen et al., Bat-infecting merbecovirus HKU5-CoV lineage 2 can use human ACE2 as a cell entry receptor, Cell (2025), https://doi.org/10.1016/j.cell.2025.01.042

luciferase activity using the *Rennila* Luciferase Assay System (Promage) and the plate was read with an Agilent BioTek Synergy H1 Multi-Mode Microplate Reader (BioTek).

RBD-hFc live-cell binding assay

HEK293 cells were transiently transfected with the respective ACE2 ortholog. After 36 h.p.t., the cells were incubated with 4 μg/mL BtHKU5-CoV-2-441 RBD-hFc recombinant proteins at 37 °C for 30 min, and subsequently incubated with 1 μg/mL of Alexa Fluor 488-conjugated goat anti-human IgG (Thermo Fisher Scientific) diluted in Hanks' balanced salt solution (HBSS) with 1% BSA at 37°C for 1 h. After washing cells with HBSS, the cell nuclei were stained with Hoechst 33342 (1:10,000 dilution in HBSS) at 37°C for 30 min. The images were captured using a fluorescence microscope (MI52-N).

Establishment of the *hACE2*-knockout cell line

The Huh-7 ACE2 KO and Caco-2 ACE2 KO cell line was constructed with the CRISPR/Cas9 editing system. The single-guide RNA sequence binding *hACE2* used in this study was: 5'-TGAGCAGGGAGGCATCCAAT-3' and 5'-TGCTGCTCAGTCCACCATTG-3'. In brief, sequence upon with an added 'G' at 5' was cloned to pLentiCRISPRv2 vector. Then the lentivirus was packaged by co-transfect with pLentiCRISPRv2, pMDLg/pRRE, pRSV/Rev and pMD2.G plasmids into HEK293 cells. Huh-7 cells were lentivirally transduced and then selected with puromycin. Surviving cells were performed flow cytometry for single clone purification. Successful *h*ACE2-knockout cell line was verified using Sanger sequencing and western blot.

Western blot

To detect S protein cleavage during biogenesis, cells were lysed and total proteins were separated by 10% sodium dodecyl sulfate-polyacrylamide gel (SDS-PAGE) electrophoresis and then transferred onto a polyvinyl difluoride (PVDF) membrane (Millipore). After SDS-PAGE and PVDF membrane transfer, the blots were blocked with 5% BSA in TBST (20 mM Tris, 150 mM NaCl, 0.1%Tween-20) supplemented with 0.05% Tween-20 at room temperature for 1 h. The membrane was incubated with the indicated primary antibodies at 4 °C overnight and the indicated secondary antibodies at room temperature for 1 h. The signals were detected using immobilon western horseradish peroxidase substrate (Millipore). For the detection of full and cleaved S protein, the membrane was incubated with mouse anti-Stag monoclonal antibody (1:5,000) and detected with horseradish peroxidase-conjugated goat anti-mouse IgG (Proteintech, 1:10,000). For the detection of human GAPDH protein, the membrane was incubated with mouse monoclonal antibody (Proteintech, 1:10,000) and detected with horseradish peroxidase-conjugated goat anti-mouse IgG (Proteintech, 1:10,000).

To assess S protein cleavage by trypsin, the supernatant containing pseudotyped virus particles bearing S protein was concentrated by a 30kD ultrafiltration tube, and the residual volum was mixed well and divided into 7 different tubes. Different concentration of trypsin (0.5 μg/mL, 1μg/mL, 2 μg/mL, 3 μg/mL, 4 μg/mL, 5 μg/mL) were added to the tubes, and no trypsin treatment was set as a control. All of the tubes were incubated at 37°C for 20 min. After incubation, 6×SDS-loading buffer was added and heated for 10 min at 100°C before SDS-PAGE and immunoblotting were performed.

Protein expression and purification

BtHKU5-CoV-2-441 RBD and human ACE2 proteins were expressed by the Bac-to-Bac Baculovirus Expression System (Invitrogen). BtHKU5-CoV-2-441 RBD were expressed in Sf9 insect cells, and human ACE2 was expressed in Hi5 insect cells. The process was as follows: (1) The insect cells (Sf9/Hi5) were cultured in the medium of SFX-Insect (Cytiva), SF900 II and Grace (Thermo Fisher Scientific) with a density of 1×10^6 cells/mL. (2) P0 generation baculovirus was amplified to obtain P1 baculovirus. The amplification process was as follows: 1 mL of P0 baculovirus was added to 50 ml of Sf9 cells, cultured in SFX-Insect, SF900 II, and Grace media, and harvested within 72 h after infection. (3) As previously mentioned, 1 mL of P1 baculovirus was added to 500 ml of Sf9/Hi5 cells and secreted BtHKU5-CoV-2-441 RBD, and human ACE2 proteins were harvested in the medium within 72 h after infection. The mutant BtHKU5-CoV-2-441 RBD proteins were expressed in HEK293F cells. Then, secreted mutant proteins were harvested in the medium within 120 h of transfection. BtHKU5-CoV-2-441 RBD and human ACE2 proteins were bound by High Affinity Ni-Charged Resin FF (GenScript). First, Ni column was washed with low-salt and low-imidazole detergent buffer (20 mM Tris-HCl, 150 mM NaCl, 4 mM $MgCl_2$, 4 mM DTT, 10%(v/v) glycerol, 20 mM imidazole) at pH 8.0. Elution buffer (20 mM Tris-HCl, 150 mM NaCl, 4 mM $MgCl_2$, 500 mM imidazole) at pH 8.0 was used to add the target protein to the Ni column several times. The eluents were used to further purified RBD and ACE2 protein samples with a Superdex 75 10/300 Increase column (GE Healthcare) or Superdex 200 10/300 Increase column (GE Healthcare) by size exclusion chromatography in PBS. Protein concentration was determined using absorption at 280 nm. The purified proteins are packaged and stored at -80°C. The BtHKU5-CoV-2 RBD-hACE2 complex was prepared by protein coupling with a ratio of 1.2:1, and incubated with 0.1% glutaraldehyde on ice for 60 minutes. The mixture is then further purified by size-exclusion chromatography via a Superdex 200 10/300 Increase column (GE Healthcare). The components containing the complex are collected and concentrated to 1 mg/mL.

SPR

The SPR technique (Biacore 8K+, Cytiva) was used to determine the binding affinity of wild-type and mutant BtHKU5-CoV-2-441 RBD to human ACE2. Wild-type and mutant RBD proteins were immobilized on Seriers S Sensor Chip CM5. Human ACE2 was then injected at a rate of 25 μl/min using single cycle kinetics with an injection time of 120 seconds per concentration followed by

a dissociation time of 300 seconds. The concentration of human ACE2 varies from 187.5 to 30,000 nM, and the surface is finally regenerated without a kinetic buffer of RBD to define the background. After fitting the experimental data to a 1:1 Langmuir binding model in Biacore 8K+ evaluation software, the binding dynamics (KD, ka, kd) were obtained.

Cryo-EM sample preparation and data collection

For low temperature EM sample preparation, the BtHKU5-CoV-2-441 RBD-hACE2 complex is diluted to 0.5 mg/mL. The copper mesh (X-100-Cu300) is freshly glowing with PELCO easiGlow™ 91000 (PELCO) for 60 seconds with current setting of 15 mA. The 4 μL mixture complex was transferred to the grid, applied with filter paper at 8°C and 100% humidity, and injected into ethane using Vitrobot Mark IV (FEI). For these complexes, Titan Krios G4 microscope (Thermo Fisher Scientific) with EPU automatic Data Collection software, equipped with Folcon 4i detector (Gatan), collects micrographs at 300 kV. The videos with total dose of 50 $e^{-}/Å^{2}$) were recorded at a final pixel size of 0.73 Å, defocusing between −0.8 and −2.0 μm.

Imaging processing

A total number of 6616 micrographs were recorded for BtHKU5-CoV-2-441 RBD-hACE2 complex. The dataset was processed using Cryosparc (Version 4.0.1). Raw data was processed using pacth motion correction of Cryosparc 4.0.1. After the raw data were aligned and averaged into motion-corrected summed images, then defocus values for each micrograph were determined using pacth CTF estimation. Next, particles were picked and extracted for multi-rounds of 2D classification. Well-defined partial particles were selected for initial model reconstruction using *ab-initio* reconstruction. The initial model was used as a reference for heterogeneous refinement. Then homogeneous refinement was preferment, and non-uniform refinement used to improve the quality of map. After refinement and post-processing, the overall resolution of the BtHKU5-CoV-2-441 RBD-hACE2 complex was up to 2.96 Å based on the gold-standard Fourier shell correlation (FSC; threshold = 0.143).

Model building and refinement

The BtHKU5-CoV-2-441 RBD-hACE2 complex structures were manually built into the refined maps using Coot (v.0.9.6). The atomic model was further refined by positional and B-factor refinement in real space using Phenix (v.1.20). N-linked glycans were manually built into the density where visible. The model was validated and analyzed using MolProbity. The figures were generated using UCSF Chimera and Chimera X. The datasets and refinement statistics are shown in Table S2.

Virus isolation

Anal swab samples from bats that had been tested HKU5-CoV-2 positive by PCR were centrifuged and diluted in MEM. The Caco-2-hACE2 cell monolayers were inoculated with 200 μL diluted samples at 34°C for 2 h. Fresh MEM containing double dose of antibiotic-antimycotic (Gibco) and 2.5 μg/mL trypsin was added to a final volume of 500 μL without removing the inoculum. The cells were incubated in a 5% CO_2 and 34°C incubator. The supernatants were absorbed every day for detecting viral amplification by quantitative reverse transcription PCR (qRT-PCR) and the cells were fixed after 5-day incubation for immunofluorescence staining. Virus was titered using a Caco-2-hACE2 cell-based infectivity assay and represented as $TCID_{50}$/mL.

Immunofluorescence staining

Cells were washed with PBS twice and fixed with 4% paraformaldehyde at 4°C overnight. Viral nucleocapsid protein (NP) was detected using an in-house rabbit polyclonal antibody against BtHKU5-CoV-2-441 NP as a primary antibody and a Cy3-anjuated goat anti-rabbit IgG (Abcam, 1:200). ACE2 expression was detected using DYKDDDDK-Tag (3B9) mouse monoclonal antibody (Abmart, 1:500) or an in-house mouse monoclonal antibody against Stag followed by Alexa Fluor 488-conjugated goat anti-mouse IgG (Abcam, 1:100), Alexa Fluor 594 conjugated goat anti-mouse IgG (Abcam, 1:200) or Alexa Fluor 594-conjugated goat anti-mouse IgG (Thermo Fisher Scientific, 1:200). Cell nuclei were stained with DAPI (5 ng/mL). Staining images were collected using a fluorescence microscope (Thermo Fisher Scientific).

Infection in human organoids

Human airway, nasal and colon organoids were trypsinized after removing the Matrigel from the organoids, and then infected with BtHKU5-CoV-2-023 at an MOI of 0.5 and incubated at 34°C for 3 h. After incubation, the organoids were washed once with PBS and centrifugated at 250× g for 3 min. The organoid pellets were embedded in Matrigel and seeded in a 24-well plate. After polymerization, culture medium was added. At the indicated time points, organoids culture media were harvested for RNA extraction and viral load quantification by qRT-PCR.

RNA extraction and qRT-PCR

Viral RNA was extracted from culture supernatants and organoids using a DNA/RNA Extaction Kit (Prepackaged, Vazyme) according to the manufacturer's instruction. Viral RNA copies were determined by one-step qRT-PCR using primers targeting BtHKU5-CoV-2-023 *RdRp* gene (forward: 5'-TCGTCAGTACCACCAGAAGA-3', reverse: 5' -CATAAAGTCCCACCCACCATAG-3') and then comparing the Ct values to a standard curve derived from a cDNA clone. One step qRT-PCR was run using the HiScript II One Step qRT-PCR SYBR Green Kit (Vazyme) on a CFX Connect Real-Time PCR Detection System (Bio-Rad).

Please cite this article in press as: Chen et al., Bat-infecting merbecovirus HKU5-CoV lineage 2 can use human ACE2 as a cell entry receptor, Cell (2025), https://doi.org/10.1016/j.cell.2025.01.042

ACE2 blocking assay

Caco-2-hACE2 cells were pre-treated with different concentration of h11B11 antibody, SARS-CoV-2 RBD protein, SARS-CoV RBD protein, MERS-CoV RBD protein and mock-treated as a control at 37°C for 2 h. After pretreatment, antibody or RBD protein was removed and BtHKU5-CoV-2-023 infected cells as an MOI of 0.01 at 34°C for 1 h. Then viral inoculum was removed and cells were washed with MEM for twice. Fresh media containing corresponding concentration of h11B11 antibody or coronavirus RBD protein were added to cells. Cells were cultured in a 5% CO_2 and 34°C incubator. At 72 h.p.i, supernatants were absorbed for detecting viral RNA concentration by qRT-PCR and the cells were fixed for immunofluorescence staining.

Protease inhibition

For the experiments using BtHKU5-CoV-2-441 pseudotyped viruses, Caco-2-hACE2 cells were incubated with 50 μM decanoyl-RVKR-CMK (Tocris), 50 μM Camostat (MedChemExpress), 50 μM E64D (Selleck), 500 nM BafA1 or 50 μM Hydroxychloroquine for 2 h before pseudotyped virus transduction. Equal volumes of dimethylsulfoxide (DMSO) served as a vehicle control. After the 2 h pretreatment, the media containing inhibitors and control media were removed. The Caco-2-hACE2 cells were transduced with BtHKU5-CoV-2-441 pseudotyped viruses in a 5% CO_2 incubator at 37 °C for 48 h and then luciferase was evaluated in the same way as described for the pseudotyped virus entry assay. For the experiments using BtHKU5-CoV-2-023 authentic viruses, Caco-2-hACE2 cells pre-treated with 100 μM Camostat (MedChemExpress), 100 μM E64D (Selleck), 100 μM Camostat (MedChemExpress) combined with 100 μM E64D (Selleck), or mock-treated, and then infected with KU5-CoV-2-023. After 2 h incubation, viruses were removed and cells were washed twice and added fresh culture media. After 72 h infection, supernatants were used to extract viral RNA and determine the viral RNA concentration by qRT-PCR and cells were fixed for immunofluorescence staining.

Neutralization assays

The neutralization efficacy of monoclonal antibodies (REN10933 and REN10987) targeting SARS-CoV-2 RBD, monoclonal antibody (m336) targeting MERS-CoV RBD, S2 antibodies (76E1 and S2P6) and peptide inhibitor (EK1C4) targeting HR1 domain of coronavirus S protein was evaluated using BtHKU5-CoV-2-441 pseudotyped viruses. The antibodies and peptide inhibitor were serially diluted (twofold or threefold) and incubated with BtHKU5-CoV-2-441 pseudotyped viruses at 37 °C for 30 min. The mixture was then transferred to a 96-well plate with Caco-2-hACE2 cells in triplicated. 24 h after transduction, luciferase activity was measured in the same way as described for the pseudotyped virus entry assay. Pseudovirus-only transduced cells were assayed as a control.

QUANTIFICATION AND STATISTICAL ANALYSIS

Data are presented as means and standard errors of the means (SEMs) of at least triplicate measurements. Statistical significance was assessed using a two-tailed Student's *t*-test in GraphPad Prism 10. $P < 0.05$ was considered statistically significant. $^{*}P < 0.05$; $^{**}P < 0.01$; $^{***}P < 0.001$; $^{****}P < 0.0001$; ns, no significant difference.

Supplemental figures

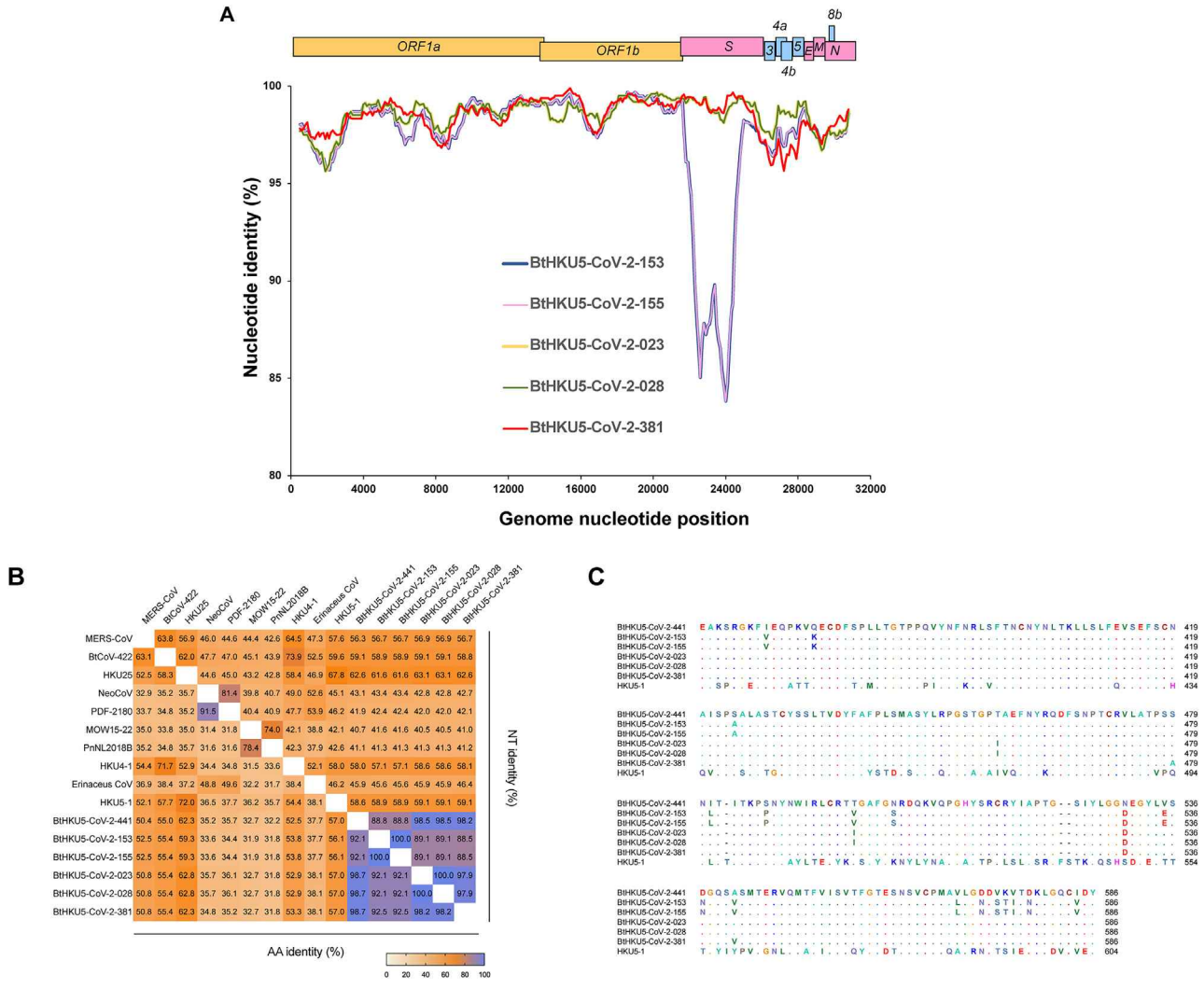

Figure S1. Comparison of BtHKU5-CoV-2 RBD with other merbecoviruses, related to Figure 1

(A) Zoomed picture for similarity plot analysis of HKU5-CoV-2 based on the full-length genome sequences. BtHKU5-CoV-2-441 was used as the query sequence. BtHKU5-CoV-2-153 and BtHKU5-CoV-2-023 are bolded.

(B) Pairwise RBD amino acid and nucleotide sequence identities of indicated merbecoviruses RBDs.

(C) RBD sequence alignment of BtHKU5-CoV-2 and HKU5-CoV-1.

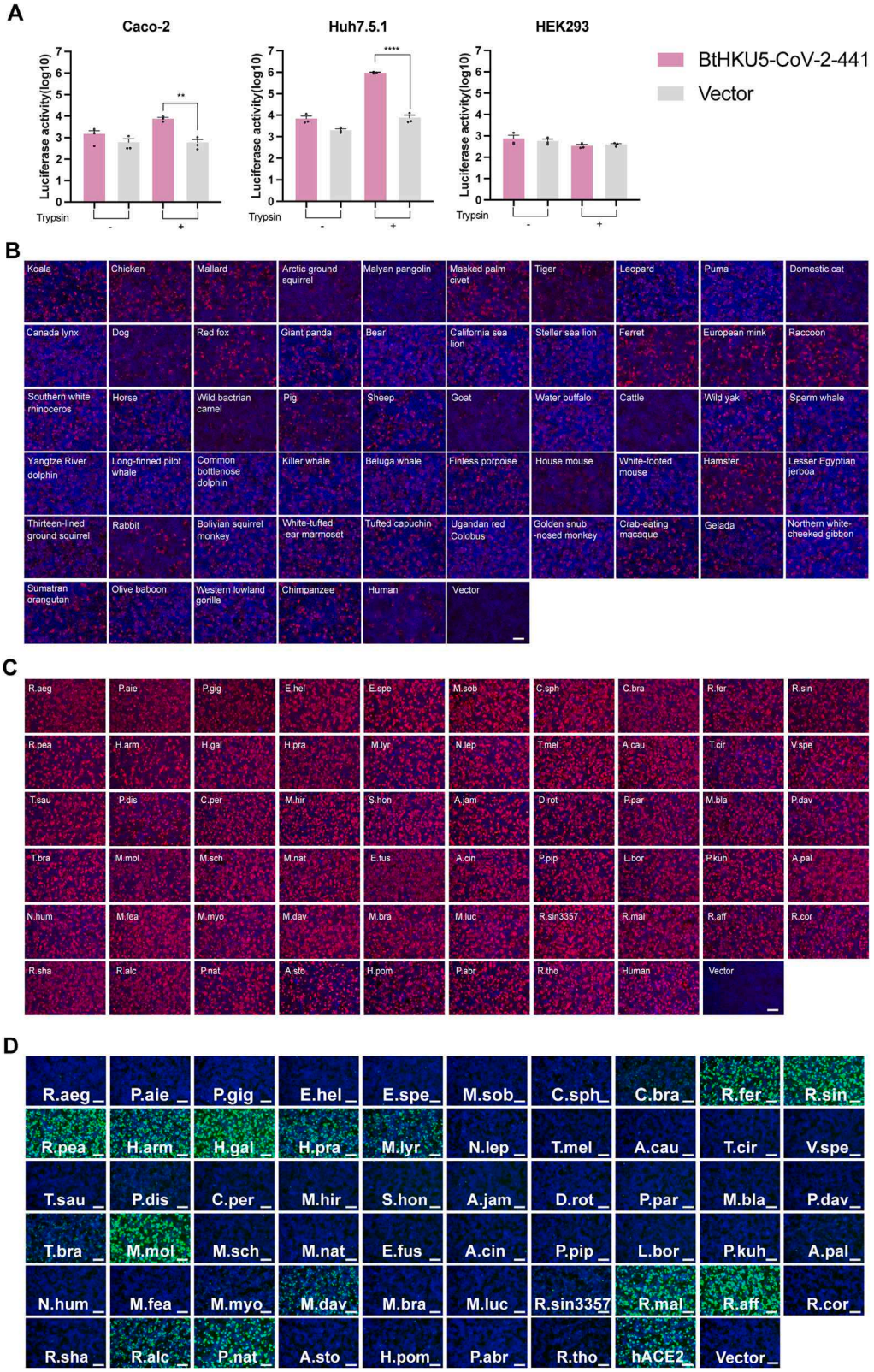

(legend on next page)

Figure S2. Cell tropism and ACE2 binding of BtHKU5-CoV-2-441, related to Figure 2

(A) Indicated cells were transduced with BtHKU5-CoV-2 pseudotyped viruses with (0.5 μg/mL) or without trypsin treatment. Entry efficiency was determined by measuring luciferase activity at 48 h.p.t.

(B and C) HEK293T cells transiently expressing 54 ACE2 orthologs from nonhuman primates, other mammals and birds and 57 bat ACE2 orthologs and fixed at 24 h.p.t. Expression of these ACE2 orthologs were tested by IFA. Scale bars, 100 μm; red, ACE2; blue, nuclei.

(D) Binding efficiency of BtHKU5-CoV-2-441 RBD to HEK293T cells transiently expressing different bat ACE2 orthologs. Scale bars, 100 μm; green, RBD binding; blue, nuclei.

Data are presented as means and SEMs of at least triplicate measurements in (A). Statistical significance was assessed using a two-tailed Student's t test.

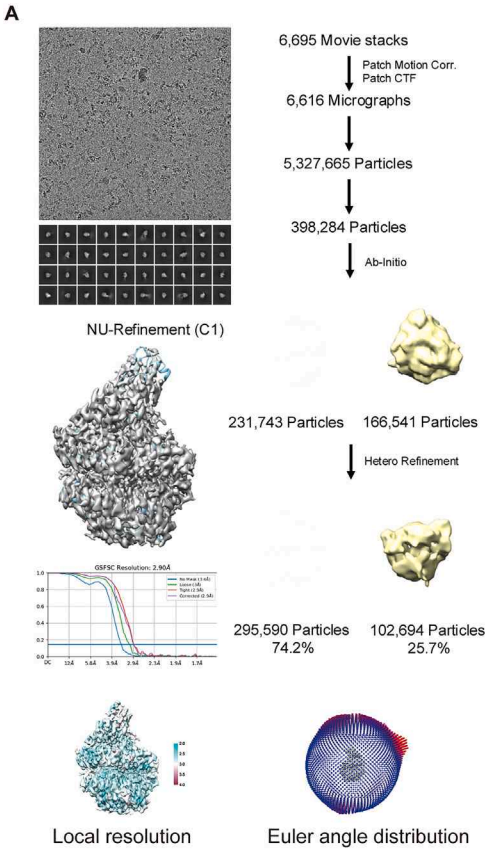

B

Patch 1		Patch 2	
BtHKU5-CoV-2-441 RBD	hACE2	BtHKU5-CoV-2-441 RBD	hACE2
R504	A387	Y448	N330
R496	E37	S453	Q325
A500(main chain O atom)	Q96	R493	Y41
S524	H34	D537	K353

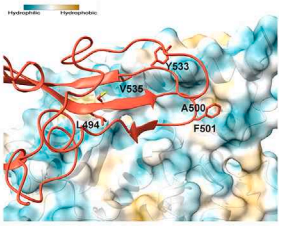

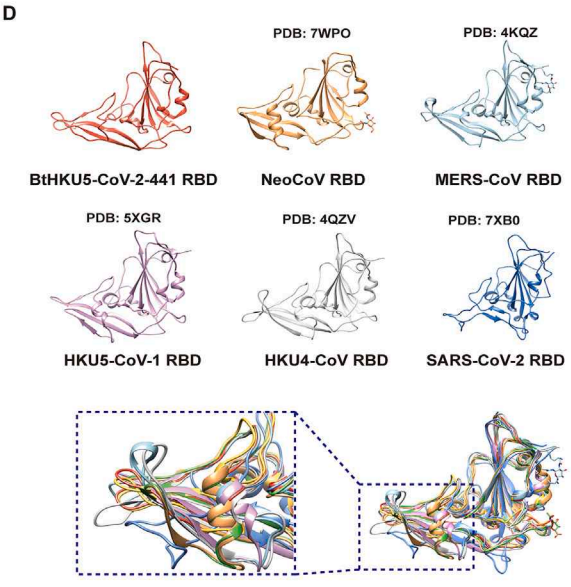

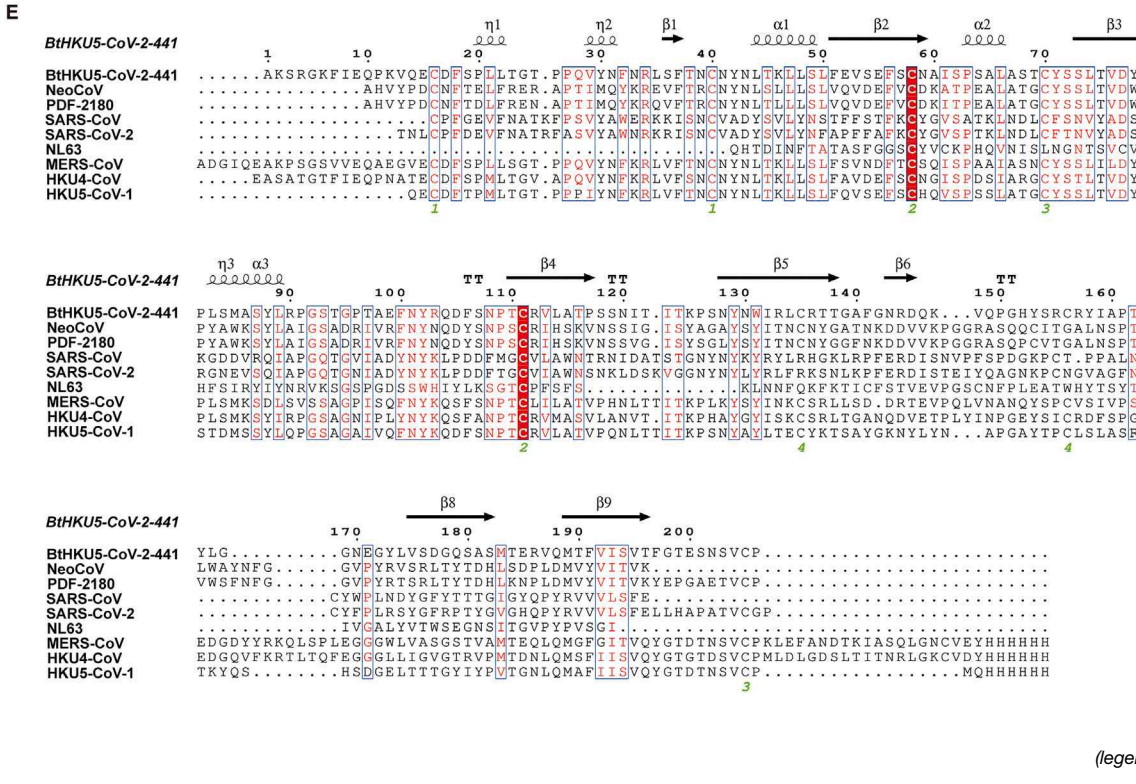

(legend on next page)

Figure S3. Interaction analysis of BtHKU5-CoV-2-441 RBD with human ACE2 and structural comparison of BtHKU5-CoV-2-441 RBD with that of different coronaviruses, related to Figure 3

(A) Cryo-EM data processing flowcharts for BtHKU5-CoV-2-441 RBD-hACE2 complex.

(B) Interaction residues between BtHKU5-CoV-2-441 RBD and human ACE2.

(C) Hydrophobic region of human ACE2 shown in ribbon representation, with interaction residues of BtHKU5-CoV-2-441 RBD displayed in stick form.

(D) Structures of BtHKU5-CoV-2-441, NeoCoV, MERS-CoV, HKU5-CoV-1, HKU4-CoV, SARS-CoV-2 RBD was shown in ribbon. The superimposition of these RBDs revealed variations in the conformations of the loops connecting β6–β9.

(E) BtHKU5-CoV-2-441 RBD sequences were aligned with those of ACE2-using and DPP4-using CoVs.

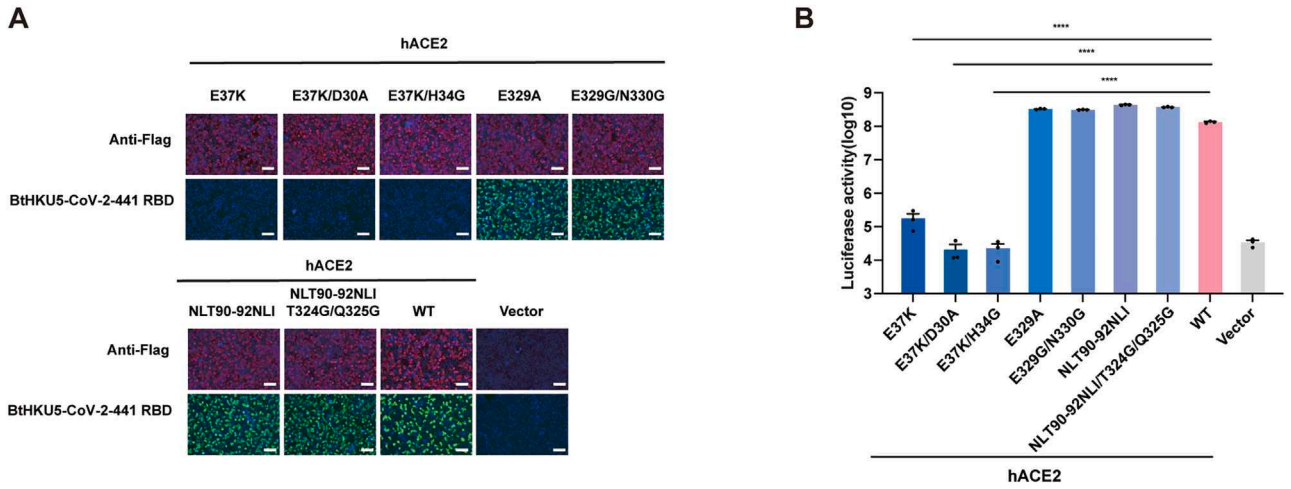

Figure S4. Effect of human ACE2 mutation on pseudotyped virus entry and RBD binding of BtHKU5-CoV-2-441, related to Figure 4

(A and B) BtHKU5-CoV-2-441 RBD binding (A: scale bars, 100 μm; green, RBD binding; blue, nuclei.) and pseudovirus entry (B) efficiency in HEK293T cells transiently expressing wild-type and mutant human ACE2.

Data are presented as means and SEMs for n=3 biological replicates in (B). Statistical significance was assessed using a two-tailed Student's t test.

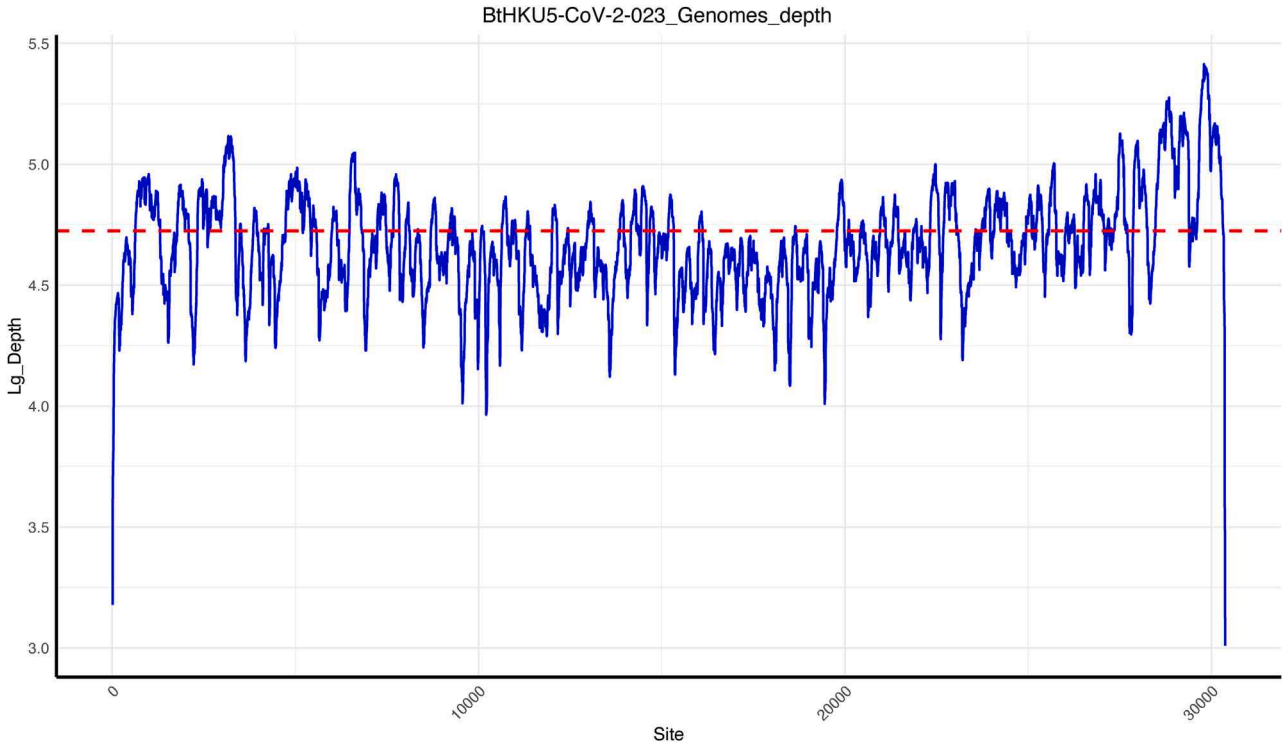

Figure S5. Mapping analysis of NGS raw reads of BtHKU5-CoV-2-023 cell culture, related to Figure 5

Viral RNA was extracted from supernatants of BtHKU5-CoV-2-023-infeted Caco-2-hACE2 cell culture and used to perform NGS. Adapters and low-quality reads were removed using fastp, and rRNA reads were removed by mapping against the SILVA rRNA database with Bowtie2. Clean reads were mapped to the reference sequence obtained from the anal swab sample, sequencing depth was shown. The red dashed line represents the mean depth of the genomes.

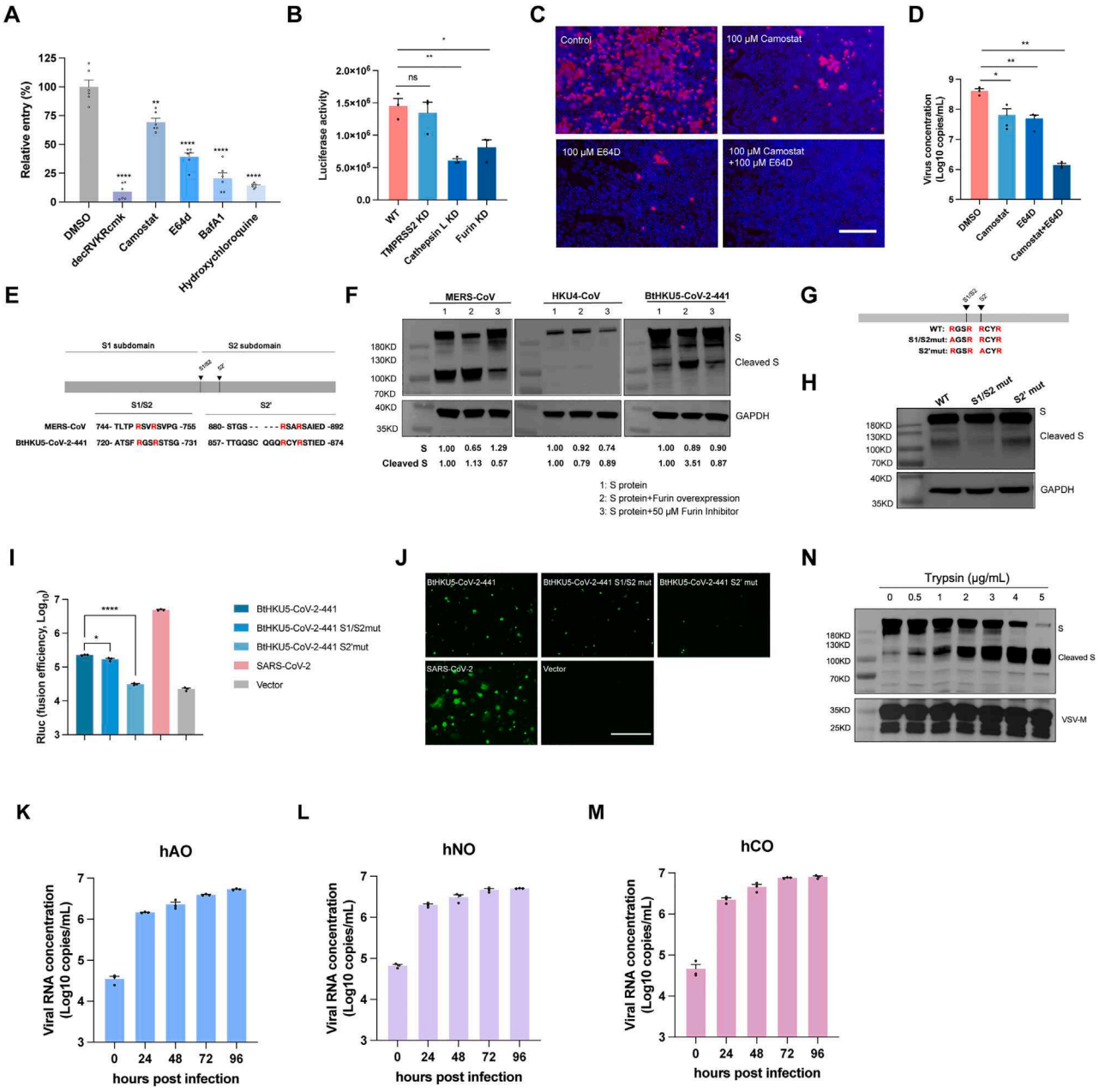

Figure S6. Effect of entry inhibitors against bat HKU5-CoV-2, related to Figure 6

(A) Effect of host protease inhibitors on cell entry of BtHKU5-CoV-2-441 pseudotyped virus. Caco-2-hACE2 cells were pretreated with indicated inhibitors for 2 h before transduction with BtHKU5-CoV-2-441 pseudotyped virus without trypsin. Viral entry was determined by measuring luciferase activity at 48 h.p.t. The cells were pretreated with 50 μM decRVKRcmk, 50 μM camostat, 50 μM E64D, 500 nM BafA1, 50 μM hydroxychloroquine, or DMSO as control.

(B) Caco-2-hACE2 cells with TMPRSS2, cathepthin L, and furin knockdown (KD) were transduced with BtHKU5-CoV-2-441 pseudotyped virus without trypsin. Viral entry was determined by measuring luciferase activity at 48 h.p.t. Entry efficiency in Caco-2-hACE2 cells were set as control.

(C and D) Effect of camostat and E64D on infection of BtHKU5-CoV-2-023 authentic virus. Caco-2-hACE2 cells were pretreated with 100 μM camostat, 100 μM E64D and the combination of 100 μM camostat and 100 μM E64D for 2 h before infected with BtHKU5-CoV-2-023 at an MOI of 0.01 without trypsin. Viral infection was analyzed by IFA (red, NP; blue, nuclei; scale bars, 300 μm) (C) and qRT-PCR (D).

(E) Schematic illustration of the coronavirus spike protein and S1/S2 and S2′ cleavage sites of indicated coronaviruses.

(F) Western blot analysis of furin-mediated S protein processing during biogenesis. BtHKU5-CoV-2-441 S protein expression plasmid was co-transfection with furin expression plasmid or empty vector into HEK293 cells, in the presence or absence of a furin inhibitor treatment. Cell lysates were collected, and S protein cleavage was analyzed through western blot. MERS-CoV and HKU4-CoV was used as positive and negative controls, respectively. Expression level of full-length S protein and cleaved S protein were quantified with ImageJ.

(legend continued on next page)

(G and H) Mutations introduced into the S1/S2 and S2′ cleavage sites in BtHKU5-CoV-2-441 S proteins and cleavage of wild-type (WT) and mutant S proteins determined by western blot analysis.
(I and J) Cell-cell fusion assay in HEK293 and HEK293-hACE2 cells mediated by WT and mutant BtHKU5-CoV-2-441 S proteins without trypsin. SARS-CoV-2 and empty vector was used as positive and negative controls, respectively. Fusion efficiencies are represented as *Renilla* luciferase activity (I) and GFP intensity (J, scale bars, 400 μm).
(K and M) Replication of BtHKU5-CoV-2-023 in human airway (K), nasal (L), and colon (M) organoids at an MOI of 0.5, measured as viral RNA copy numbers in culture media.
(N) Western blot analysis of BtHKU5-CoV-2-441 S protein on pseudotyped virus particles with or without trypsin treatment.
Data are presented as means and SEMs of at least triplicate measurements in (A), (B), (D), (I), and (K)–(M). Statistical significance was assessed using a two-tailed Student's t test. In (A), all inhibitor treated columns are compared with DMSO treated column, respectively.

Cell, Volume *188*

Supplemental information

Bat-infecting merbecovirus HKU5-CoV lineage 2 can use human ACE2 as a cell entry receptor

Jing Chen, Wei Zhang, Yang Li, Chen Liu, Tianyi Dong, Huiyu Chen, Chunguang Wu, Jia Su, Bei Li, Wei Zhang, Ben Hu, Jingkun Jia, Cheng-Bao Ma, Yan Zhu, Xiangyang He, Ang Li, Kaiyi Pan, Haofeng Lin, Zishuo Guo, Cong Li, Libiao Zhang, Huan Yan, Peng Zhou, Wei Peng, and Zheng-Li Shi

Table S1 Genome comparison of BtHKU5-CoV-2-441 with lineage 2 HKU5-CoVs and other representative merbecoviruses, related to Figure 1.

Sequence identities with Merbecoviruses (nt or aa identities %)

	5 conserved domains (aa)	Full-length genome (nt)	ORF1a (aa)	ORF1b (aa)	S1 (aa)	S2 (aa)	ORF3 (aa)	ORF4a (aa)	ORF4b (aa)	ORF5 (aa)	E (aa)	M (aa)	N (aa)	ORF8b (aa)
MERS-CoV	89.9	68.2	64.4	90.1	53.8	71.7	34.6	37.3	22.9	56.8	69.5	80.8	69.4	66.1
BtCoV-422	90.2	68.7	65.1	90.4	55.6	76.6	29.9	43.2	21.4	56.8	70.7	80.7	70.4	58.5
HKU25	89.6	68.5	64.1	90.3	58.2	76.3	36.5	39.8	26.8	55.9	69.5	77.2	68.5	58
NeoCoV	90.2	68.2	64.8	90.4	46.9	73.5	36.5	36.4	21.9	56.3	73.2	82.2	70.3	61.5
PDF-2180	90.2	68.2	65.9	90.1	47.3	73.5	40.2	37.3	21.2	56.3	69.5	80.8	72	58.5
MOW15-22	90.8	68.1	66.6	90.8	44.2	71.4	38.5	51.6	23.6	61.3	68.3	78.5	69.8	58
PnNL2018B	90.8	68.1	66.6	90.8	44.4	72.1	38.8	51.6	23.9	62.2	68.3	78.1	69.7	58.5
HKU4-1	90.3	71.3	70.7	89.3	54.3	75.7	37.9	49.6	32.3	46.6	79.3	81.3	75.1	54.4
Erinaceus CoV	86.5	64.5	59.2	86.8	44.9	67.4	24.5	40	19.3	45.9	61	76.1	65.6	42.6
HKU5-1	95.1	78.9	81	94.4	57.4	81.5	68.6	59.7	45.5	66.1	95.1	86.3	81.1	65.4
BtHKU5-CoV-2-153	99.7	97.5	98.4	99.8	91.2	99	99	93	94.7	98.7	100	99.1	99.3	92.1
BtHKU5-CoV-2-155	99.7	97.5	98.4	99.8	91.2	99.2	99	93	94.7	98.7	100	99.1	99.3	92.1
BtHKU5-CoV-2-023	99.6	98.5	98.8	99.6	98.6	99.7	99	98.2	97.9	97.8	100	99.1	99.3	92.7
BtHKU5-CoV-2-028	99.6	98.5	98.8	99.6	98.6	99.7	99	98.2	97.9	97.8	100	99.1	99.3	92.7
BtHKU5-CoV-2-381	99.9	98.4	98.7	99.9	99.2	99.7	98	93.7	95.4	97.3	100	99.5	99.1	94.2

Table S2 Cryo-EM data collection, refinement and validation statistics, related to Figure 3.

	BtHKU5-CoV-2-441 RBD-hACE2
Data collection and processing	
Magnification	139,000
Voltage(kV)	300
Electron exposure(e-/Å^2)	50
Defocus range (μm)	-0.8 ~ -2.0
Pixel size (Å)	0.73
Symmetry imposed	C1
Initial particle images (no.)	398,294
Final particle images (no.)	295,590
Map resolution (Å)	2.90
FSC threshold	0.143
Map resolution range (Å)	Infinity ~ 2.90
Refinement	
Initial model used (PDB code)	none
Model resolution (Å)	2.96
FSC threshold	0.143
Map sharpening B factor (Å^2)	-122.5
Model composition	
Non-hydrogen atoms	6351
Protein residues	771
Ligands	9
B factors (Å^2)	
Protein	56.95
Ligands	92.72
R.m.s derivations	
Bond lengths(Å)	0.003
Bond angles (°)	0.532
Validation	
MolProbity score	1.48
Clashscore	7.81
Poor rotamers(%)	0.88
Ramachandran Plot	
Fvaored (%)	97.70
Allowed (%)	2.33
Disallowed (%)	0.00

Table S3 Residues of BtHKU5-CoV-2-441 RBD interaction with human ACE2 at binding interface (using a cutoff distance of 4.5 Å), related to Figure 3.

BtHKU5-CoV-2-441 RBD	Human ACE2	BtHKU5-CoV-2-441 RBD	Human ACE2
S447	Q325	F501	K26
	E329		N90
Y448	Q325		T92
	E329		V93
	N330		P389
S453	Q325	G502	A387
T454	N322		Q388
	M323		P389
	T324	N503	A387
	Q325		Q388
G455	T324		P389
P456	T324		F390
	K353		R393
	G354	R504	A387
R493	Y41	S524	H34
	K353	Y526	T27
	D355		D30
L494	K353	G529	D30
	G354	G532	D30
R496	A386	Y533	D30
	E37		K31
	K353		H34
	G354	V535	H34
T498	D30		E37
	H34		D38
	E37		K353
G499	D30	D537	Y41
	N33		K353
A500	K26		
	L29		
	D30		
	N33		
	Q96		
	P389		